

First-principles study of ferroelectric oxide epitaxial thin films and superlattices: role of the mechanical and electrical boundary conditions

Javier Junquera

*Departamento de Ciencias de la Tierra y Física de la Materia Condensada,
Universidad de Cantabria, Avda. de los Castros s/n, E-39005 Santander, Spain*

Philippe Ghosez

Physique Théorique des Matériaux, Université de Liège, B-4000 Sart Tilman, Belgium

(Dated: February 9, 2022)

Abstract

In this review, we propose a summary of the most recent advances in the first-principles study of ferroelectric oxide epitaxial thin films and multilayers. We discuss in detail the key roles of mechanical and electrical boundary conditions, providing to the reader the basic background for a simple and intuitive understanding of the evolution of the ferroelectric properties in many nanostructures. Going further we also highlight promising new avenues and future challenges within this exciting field or researches.

To appear in "*Journal of Computational and Theoretical Nanoscience*"

Keywords: ferroelectricity, perovskite oxides, size effects, thin films, superlattices, nanowires, nanoparticles, mechanical boundary conditions, strain, electrical boundary conditions, depolarizing field

I. INTRODUCTION

During the recent years, numerous studies have been reported in the field of ferroelectric oxide nanostructures. These were motivated by the perspective of new technological applications and made possible thanks to combined spectacular developments of experimental and theoretical techniques.¹ On the experimental side, it is now possible to grow oxide nanostructures with a control at the atomic scale and to measure their properties using local probes. On the theoretical side, different significant advances have been realized in the field of first-principles calculations that, combined to the recurrent increase of computational power, allow not only to reproduce accurately experimental measurements but also to make trustable predictions that are verified a posteriori.

The study of ferroelectric nanostructures is nowadays a broad field of researches and it would be impossible to provide an exhaustive description of earlier works in a short review paper. Our purpose here is to provide a simple and comprehensive description of the origin of ferroelectric finite size effects and to highlight some recent results, focusing essentially on epitaxial thin films and superlattices. For a more complete and detailed description of recent first-principles achievements concerning ferroelectrics and their nanostructures, we refer the reader to recent book chapters^{2,3,4} and topical review papers.^{5,6,7,8,9,10}

In the present review, we focus our attention on the influence of mechanical and electrical boundary conditions. Although other effects might also be important (chemistry of interfaces, defects ...), both effects play a key role and already allow to understand the main ferroelectric finite size effects when properly taken into account. The roles of mechanical and electrical boundary conditions are introduced separately and their respective influence is first illustrated in the paradigmatic case of a BaTiO_3 (the standard ferroelectric perovskite oxide material, see Sec. II) thin film under realistic conditions, including its epitaxial growth on SrTiO_3 (Sec. III A), and the screening of its polarization charge by realistic electrodes (Sec. III B). Once the basic physical effects have been introduced, the discussion is enlarged to other perovskite oxides epitaxial films (Sec. III C) and superlattices (Sec. IV). Finally, recent works on other types of ferroelectric oxide nanostructures, such as nanoparticles or nanowires, are briefly reviewed (Sec. V).

II. BACKGROUND

Barium titanate (BaTiO_3) is a prototypical ferroelectric oxide.¹¹ At high temperature, it is paraelectric and crystallizes in the high-symmetry cubic perovskite structure as illustrated in Fig. 1a: Ba atom is located at the corner of the cubic unit-cell while the Ti atom is at the center and is surrounded by an octahedra of O atoms, themselves located at the center of each face of the cube. On cooling, BaTiO_3 undergoes a sequence of three ferroelectric phase transitions to structures successively of tetragonal ($T_c \approx 130^\circ\text{C}$), orthorhombic ($T_c \approx 5^\circ\text{C}$) and rhombohedral ($T_c \approx -90^\circ\text{C}$) symmetry. In the following discussion, we will focus on the tetragonal phase that is stable at room temperature.

The phase transition from cubic to tetragonal is characterized by the opposite shift of Ti and O atoms with respect to Ba, taken as reference. This polar atomic distortion is accompanied with a small relaxation of the unit cell and yields a stable spontaneous polarization of $26 \mu\text{C}/\text{cm}^2$ at room temperature. In the tetragonal phase, the cubic symmetry is broken, resulting not in a unique polar structure but in six symmetrically equivalent variants with polarization along the $[100]$, $[010]$ and $[001]$ directions. The two variants along $[001]$ (“up” and “down” states) are represented in Fig. 1a. What makes BaTiO_3 ferroelectric is not only the existence of energetically equivalent polar states but also the fact that it is possible to switch from one to another of these states by applying an electric field larger than the coercive field. Related to this switchability, the relationship between polarization and electric field is hysteretic in ferroelectrics, as illustrated in Fig. 1c.

In what follows, the pattern of cooperative atomic displacements associated to the phase transition will be referred to as ξ , and the paraelectric, up and down states respectively will be labeled as ξ equal to 0, 1 and -1 respectively. For continuous evolution of ξ , the internal energy U of the crystal has a typical double-well shape illustrated in Fig. 1b. In BaTiO_3 , the well depth is typically of the order of $30 \text{ meV}/\text{cell}$. While hysteresis loops (Fig. 1c) constitutes the measurement of choice to demonstrate experimentally ferroelectricity, the existence of a double-well shape for the energy is usually considered as the theoretical fingerprint of the ferroelectric instability. Making a Taylor expansion of U in terms of ξ around the paraelectric state taken as reference, and since the odd terms are forbidden by symmetry, we can write

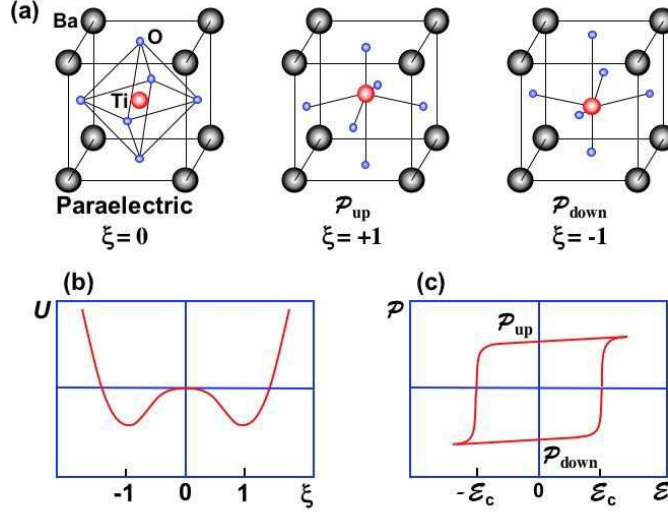


FIG. 1: (a) Crystal structure of BaTiO₃ in its high temperature paraelectric cubic perovskite structure and in its room temperature tetragonal structure (for “up” and “down” polarization states). (b) Typical double-well shape for the internal energy of BaTiO₃ in terms of ξ (see text). (c) Hysteretic behavior of the polarization-electric field curve. Figure taken from Ref. 2.

$$U(\xi) = A\xi_z^2 + B\xi_z^4 + C\xi_z^6 + D\xi_z^8 + \dots, \quad (1)$$

where for the sake of simplicity we have assumed that atomic displacements in the tetragonal phase can take place only along z (condition that will be held all along this review unless otherwise stated), and we have cut the expansion in the eighth power of the atomic pattern of displacement. U presents a typical double-well shape with a negative curvature at the origin so that, in the previous equation, ferroelectricity can be associated to a negative value of A ($A < 0$). We note that, in the limit of a homogeneous polarization, the previous expansion in terms of microscopic atomic variable ξ is similar in spirit to that of Devonshire-Ginzburg-Landau (DGL) phenomenological theory^{12,13} in terms of the macroscopic polarization, since

$$P_z \approx (1/\Omega_0)Z_{zz}^*\xi_z, \quad (2)$$

where Ω_0 is the unit cell volume and Z_{zz}^* is the diagonal component of Z^* , the effective charge tensor associated to ξ , so that part of the foregoing discussion can be transposed in that alternative context.

At the bulk level, a coherent microscopic model explaining the origin of ferroelectricity was first reported by Cochran,¹⁴ who identified an intimate link between the structural phase transition and the lattice dynamics and introduced the concept of soft mode. Specifically, the underlying idea is that the lowest-frequency zone-center polar phonon mode in the paraelectric phase becomes softer as a function of decreasing temperature, and finally goes down to zero frequency, freezing in below T_c to generate the ferroelectric crystal structure. Cochran's theory of displacive phase transition was exhibited in the context of a shell-model and the softening of a given polar mode was explained from a competition between short-range and long-range Coulomb interactions.

Most of these ideas were further confirmed from first-principles calculations³ performed within the density functional theory (DFT). An unstable polar mode (i.e. a mode with imaginary frequency ω within the harmonic approximation) has been identified at Γ in the paraelectric phase of various ferroelectric oxides¹⁵ and, in prototypical cases like BaTiO₃, a strong resemblance has been observed between the eigendisplacement vector of this unstable phonon and the ground-state distortion ξ (overlap of 99 % in BaTiO₃ or LiNbO₃¹⁶). Since energy curvature is related to the square of the frequency, an unstable mode with imaginary frequency in the paraelectric phase is the indication of a negative curvature of the energy at the origin [$A < 0$ in Eq. (1)]. The amplitude of ω does not directly provide the double-well depth that additionally depends on anharmonic effects but measures, to some extent, the strength of the instability. The origin of the ferroelectric instability was also investigated at the first-principles level and the competition between short-range (SR) interactions and long-range (LR) Coulomb forces has been confirmed and quantified.¹⁷ In this context, the anomalous values of the Born effective charges of ferroelectric oxides^{15,18} was shown as an essential feature to produce an unusually large destabilizing Coulomb interaction responsible for the ferroelectric instability.

The balance of forces resulting in the ferroelectric instability is also well-known to be strongly sensitive to strain and external pressure. The sensitivity of the ferroelectric distortion to strain is inherent to the piezoelectric behavior and was highlighted from the early stage of first-principles computations.^{19,20} Samara *et al.*²¹ proposed that external hydrostatic pressure reduces and eventually totally suppresses ferroelectricity since SR repulsions increases more rapidly than LR destabilizing forces under pressure. This latter result was recently reinvestigated at the first-principles level,^{22,23} confirming a rapid disappearance of

ferroelectricity at moderate pressure and additionally pointing out an unexpected recovery of ferroelectricity at extremely high pressure.

Such microscopic understanding of ferroelectricity at the bulk level allows to anticipate the existence of strong finite size effects in ferroelectrics since both SR and LR forces will be modified in nanostructures. The SR forces will be modified at surface and interfaces due to the change of atomic environment. The same is true for the Born effective charges that cannot keep their bulk value²⁴ as it was illustrated on BaTiO₃ thin films by Fu and coworkers.²⁵ Beyond that, the LR Coulomb interaction will be cut because of the finite size of the sample and will be strongly dependent on the electrical boundary conditions. Finally, since the ferroelectric instability is strongly sensitive to strains, it will be influenced by mechanical boundary conditions such as epitaxial strains.²⁶

These different factors can act independently to either enhance or suppress ferroelectricity. They will compete with each other in such a way that it is difficult to predict the ferroelectric properties of nanostructures without making explicit investigations.

III. EPITAXIAL THIN FILMS

During the recent years, most of the efforts devoted to understanding ferroelectric finite size effects concerned ferroelectric thin films. This was partly motivated by the observation at the end of the nineties of a polar ground-state in ultrathin films^{27,28} with thicknesses well below 10-20 nm, that was still considered at that time as a realistic estimate of critical thickness for ferroelectricity.²⁹

It is now understood that the survival or disappearance of ferroelectricity in ultrathin films is not a truly intrinsic property: it strongly depends on the structure and chemistry of the interface between the ferroelectric and the substrate and/or the electrodes as well as on electrical (e.g. screening of the depolarizing field) and mechanical (e.g. epitaxial strains) boundary conditions. On top of that, additional features such as the finite conductivity of the film or the presence of structural defects and vacancies might also affect the ferroelectric properties. Although these latter features are potentially important, the proper treatment of their effect remains beyond the scope of first-principles simulations and is not yet fully understood so that these effects will not be further discussed here. For an overview of atomic relaxations and discussions of the stability of surfaces and interfaces we refer the reader to

previous reviews.^{2,5,9} In what follows, we will restrict the discussion on the role of mechanical and electrical the boundary conditions which, in most cases, provide a sufficient background to achieve relevant understanding of observed ferroelectric finite size effects.

A. Mechanical boundary conditions : the epitaxial strain

As mentioned in Sec. II, ferroelectricity in bulk compounds is well-known to be very sensitive to strains.^{11,19} In thin films, it is therefore expected that epitaxial strains will play an important role to monitor the ferroelectric properties. Coherently with that, strain engineering of the ferroelectric properties has been recently demonstrated experimentally: a polarization 250% higher than in bulk single crystals has been reported in BaTiO₃ epitaxial films,³⁰ and room temperature ferroelectricity has even been induced by strain in epitaxial SrTiO₃ thin films.³¹

In order to understand these effects, let us generalize our expansion of the internal energy in terms of additional strain e_{ij} (where i and j are cartesian directions) degrees of freedom. In our paradigmatic example of a BaTiO₃ film epitaxially grown on a (001) cubic SrTiO₃ substrate we have mixed strain/stress boundary conditions: on the one hand the in-plane strains $e_{xx} = e_{yy}$ are fixed by the lattice mismatch between BaTiO₃ and SrTiO₃, while $e_{xy} = 0$; on the other hand, the out-of-plane strain e_{zz} and the shear strains e_{xz} and e_{yz} are free to relax (condition of zero stress: $\sigma_{zz} = \sigma_{xz} = \sigma_{yz} = 0$). Again, assuming for simplicity only an homogeneous polarization along z -direction, vanishing shear strains, and restricting the expansion to leading orders in ξ and e , the free energy functional to be minimized now reads

$$\begin{aligned}
 U(\xi, e) = & A\xi_z^2 + B\xi_z^4 + C\xi_z^6 + D\xi_z^8 \\
 & + \frac{1}{2}C_{11}(2e_{xx}^2 + e_{zz}^2) + \frac{1}{2}C_{12}(2e_{xx}^2 + 4e_{xx}e_{zz}) \\
 & + 2g_0e_{xx}\xi_z^2 + (g_0 + g_1)e_{zz}\xi_z^2.
 \end{aligned} \tag{3}$$

The terms in the first line correspond to the double-well energy of Eq. (1). The terms in the second-line are the elastic energy while the terms in the third line arise from the coupling between ionic and strain degrees of freedom. They correspond to the so-called “polarization-strain coupling” and are at the origin of the piezoelectric response. It is clear from Eq.

(3) that the polarization-strain coupling terms are responsible for a renormalization of the quadratic part of U that now takes the form

$$[A + 2g_0e_{xx} + (g_0 + g_1)e_{zz}]\xi_z^2. \quad (4)$$

Depending of the value of the parameters g_0 and g_1 , and of e_{xx} and e_{zz} (deduced from the relation $\partial U/\partial e_{zz} = 0$ which follows from the boundary condition $\sigma_{zz} = 0$), we see that, playing properly with the epitaxial strain conditions, it is possible to modulate the coefficient of ξ^2 in order to increase (resp. decrease) its negative value and therefore enhance (resp. suppress) the ferroelectric character of the film.

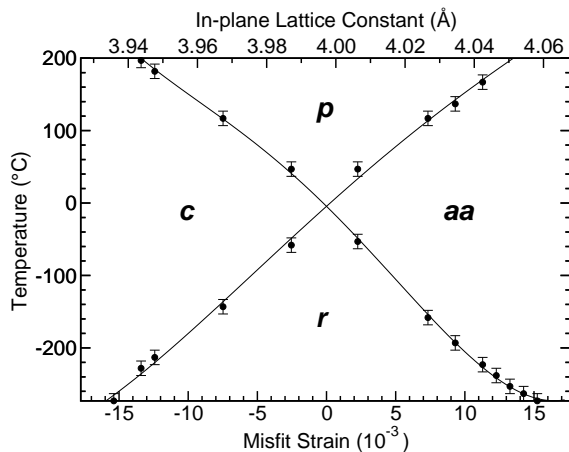


FIG. 2: Phase diagram of BaTiO₃ in terms of temperature and epitaxial misfit strain. The notation established by Pertsev *et al.*³² is followed: $p \equiv$ paraelectric phase; $r \equiv$ monoclinic phase, related with the rhombohedral bulk phase; $c \equiv$ tetragonal phase with an out-of-plane polarization along the normal; $aa \equiv$ orthorhombic phase with the polarization along the cube face diagonal perpendicular to the normal. Figure taken from Ref. 26.

The simplified free energy U in Eq. (3) can be generalized to include other orientations of ξ as well as shear strains and the different parameters can be directly determined from DFT calculations at the bulk level.^{20,33} The coefficients of the expansion for a series of ferroelectric perovskites have been reported by Diéguez *et al.*³³ These energy parametrizations at 0 K are the starting point for the development of model hamiltonians,^{34,35} that combined with classical Monte Carlo simulations allow the first-principles based studies of temperature versus strain phase diagrams in perovskite oxide films, as illustrated for BaTiO₃ on a cubic (001)

substrate in Fig. 2. Although effects such as free top surface relaxation or interaction with the substrate are neglected, the phase sequence and the topology of the phase diagram are usually well reproduced within this approach. The predicted phase transitions temperatures are however typically too low compared to those experimentally measured.

Alternatively, and in fact first applied to perovskites by Pertsev and coworkers³² before first-principles investigations, similar phase diagram can be obtained from phenomenological Devonshire-Ginzburg-Landau (DGL) type expansion of the free energy in terms of polarization and strain. Results have for instance been reported for BaTiO₃,^{30,32,36} PbTiO₃,³² SrTiO₃,^{31,37,38} and Pb(Zr_xTi_{1-x})O₃ (PZT) solid solution.³⁹ This provides more direct access to the temperature behavior and gives very accurate results around the temperature/strain regime in which the model parameters were fitted (usually near the bulk ferroelectric transition). In distant strain-temperatures regimes their predictions might be less accurate, however. For large strains or low temperatures the uncertainty increases and, as reported for BaTiO₃, different sets of DGL parameters can provide phase diagrams qualitatively different far from the bulk transition region.^{32,36}

As a general rule for the usual perovskites on a (001) substrate,²⁶ sufficiently large epitaxial compressive (resp. tensile) strains will favor a ferroelectric *c*-phase (resp. *aa*-phase) with out-of-plane (resp. in-plane) polarization while distinct behaviors are predicted for the different compounds in the intermediate regime. Of course, there might be some discrepancies with this rule, such as the one pointed by Catalan and coworkers⁴⁰ on PbTiO₃ films under tensile strains.

For the BaTiO₃ film on a (001) SrTiO₃ substrate previously considered, the large compressive epitaxial strain (-2.38 %) will strongly increase the ferroelectric phase transition temperature and favor a tetragonal *c*-phase with an out-of-plane polarization. As further estimated by Neaton and Rabe,^{41,42} such epitaxial constraint should enhance the polarization at 0 K by more than 50 %. The sensitivity of polarization to strain is however not expected to be always so large: in highly polar Pb-based systems such as Pb(Zr_xTi_{1-x})O₃ and PbTiO₃ where the ferroelectric displacements are already large, it was reported to be much more reduced than in BaTiO₃,⁴³ similarly to what was also discussed for BiFeO₃ and LiNbO₃.^{44,45}

In Ref. 26, like in many studies, the phase diagrams were obtained restricting the investigation to the effect of the epitaxial strain on the ferroelectric degree of freedom ξ , or equivalently P . In systems where different kinds of instabilities coexist (such as ferroelectric

and antiferrodistortive instabilities in SrTiO_3 ,⁴⁶ or the interplay between in-plane ferroelectricity, antiferroelectric and antiferrodistortive distortions in PbTiO_3 free standing slabs⁴⁷) the epitaxial strain can modify the competition between these instabilities so that all of them must be explicitly considered and generate much more complicated phase diagrams.⁴⁸ Also, up to now, DFT calculations were restricted to mono-domain configurations while much complex domain structures can appear as highlighted using a DGL approach^{49,50} or an effective Hamiltonian approach^{7,51} as it will be further illustrated in Section III C.

The effects imposed by the substrate on the lattice constant and geometry of the thin films can be maintained only up to a critical thickness, h_c , above which the elastic deformation can not be maintained any longer. Above h_c the strain energy is relaxed by the formation of misfit dislocations at the film-substrate interface. An estimate of h_c can be obtained using the Matthews-Blakeslee formula.⁵² A priori, this structural limit imposes some restriction on the potential enhancement of the ferroelectric properties by the mechanical boundary conditions. However, it has been found that a coherent strain state can be preserved well above the theoretical critical thicknesses expected for strain relaxation.³⁰ Moreover, in some cases, it was reported that the ferroelectric transition temperature still has a value much larger than in bulk, even after the relaxation of the strain state.⁵³

In all previous approaches, only the presence of an homogeneous strain was considered. However, “flexoelectric” coupling of a strain gradient to the polarization,^{54,55} and the related coupling of strain to a polarization gradient is receiving increasing attention. Although the characteristic scale of the flexoelectric coefficient is extremely small, it might affect the ferroelectric transitions in thin films. The subtleties of defining flexoelectric coefficients as a bulk property^{56,57,58,59} and its computation in a first-principles framework is a challenge for theoreticians.

A more exhaustive discussion of strain effects can be found in a recent topical review by K. M. Rabe.⁶

B. Electrical boundary conditions : the depolarizing field

As it was explained in Sec. II, ferroelectricity in perovskite oxides at the bulk level is a collective effect resulting from a delicate balance between SR interactions, that favour a paraelectric phase, and LR dipole-dipole electrostatic interactions, that favour a ferroelectric

distortion. So, it is expected that cutting these LR interactions by reducing the number of dipoles to interact with in a finite system, will affect the ferroelectric behavior of the material.

If we try to induce a homogeneous out-of-plane polarization in a (001) free standing BaTiO₃ slab in vacuum, preservation of the normal component of the electric displacement field at the interface will induce a depolarizing field $\mathcal{E}_d = -P/\varepsilon_0$, where ε_0 is the permittivity of vacuum (unless otherwise stated we will use throughout this review the SI system of units). This depolarizing field totally suppresses the possibility of stabilizing an homogeneous monodomain configuration with an out-of-plane polarization.

Many applications rely on films with a uniform switchable out-of-plane polarization. So, after the previous discussion, it is clear that, to stabilize such a configuration, we need to screen the depolarizing field \mathcal{E}_d . This can be achieved through two basic mechanisms: the first one is the compensation by “free” charges provided either by a metallic electrodes, semiconducting substrates, or even by ionic adsorbates^{60,61} (including in this category the screening by external applied fields that might be generated by the free charges or dipole layers);⁶² the second one, and the only one if the substrate is an insulator,^{63,64} is the breaking up of the system into 180° domains. Most of the fully first-principles calculations have been devoted to the screening by free charges, especially due to the very demanding computational effort that an explicit treatment of the domains implies, so that only the first issue will be discussed in more details here.

In an early first-principles paper, Ghosez and Rabe,⁶⁵ using a model Hamiltonian approach, showed that ferroelectricity might be preserved in ferroelectric slabs if \mathcal{E}_d is perfectly compensated. This was further confirmed by Meyer and Vanderbilt, at least for some terminations of the free standing slabs, in a fully first-principles atomistic calculation.⁶²

In principle, this total compensation of the depolarizing field could be achieved introducing the ferroelectric film between two metallic electrodes in short-circuit. However, following an idea introduced in the early seventies by Batra,^{66,67,68} Metha⁶⁹ and coworkers in the context of a phenomenological model (see Fig. 3), Junquera and Ghosez⁷⁰ demonstrated from first-principles that, even in that case, compensation of the depolarizing field is incomplete, due to the finite screening-length at the metal/ferroelectric interface.

Within this model, if a BaTiO₃ film gets a polarization normal to the ferroelectric/electrode interface, then the discontinuity of the polarization at the interface gives rise to a net interface charge density σ_{pol} ⁷² (Fig. 3a). In order to compensate for this polarization

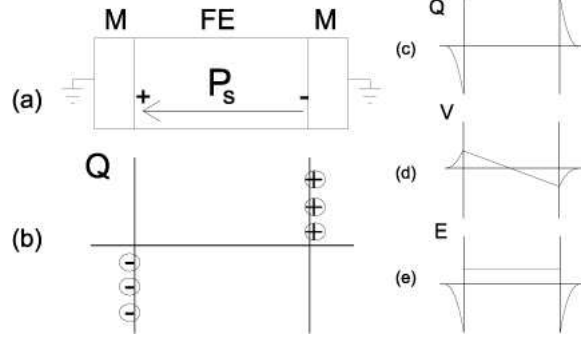


FIG. 3: A schematic diagram of (a) a short-circuited electrode-ferroelectric structure with the spontaneous polarization displayed; (b) the screening charge distribution in the presence of perfect electrodes; its (c) charge distribution, (d) voltage and (e) field profiles in the presence of realistic electrodes. Please, note that here the film is taken to be a perfect insulator. Figure taken from Ref. 71.

charge density, a screening charge is induced in the electrode that spreads in practice over a finite distance from the interface (Fig. 3c), giving rise to an interface dipole moment density and a jump in the electrostatic potential at each ferroelectric/electrode interface (Fig. 3d). This potential drop ΔV is shown to be proportional to the polarization⁷⁰

$$\Delta V = \frac{\lambda_{eff}}{\varepsilon_0} P, \quad (5)$$

where λ_{eff} is a constant of proportionality hereafter referred to as the effective screening length. Assuming a capacitor with two similar metal/ferroelectric interfaces, the total potential drop into the electrode/ferroelectric/electrode heterostructure amounts to $2\Delta V$. If the electrodes are in short-circuit (i.e. at the same potential), a residual field within the ferroelectric must compensate for this drop of potential (Fig. 3e),

$$\mathcal{E}_d = -\frac{2\Delta V}{ma_0}, \quad (6)$$

where ma_0 is the film thickness in terms of the number m of unit cells of the ferroelectric perovskite oxide. Inserting now Eq. (5) into Eq. (6)

$$\mathcal{E}_d = -\frac{2\lambda_{eff}P}{\varepsilon_0 ma_0}. \quad (7)$$

This shows that the field produced by the screening charge within the metal does not fully compensate for the bare depolarizing field $\mathcal{E}_d = -P/\varepsilon_0$: a residual depolarizing field remains that is proportional to P and to the ratio between the effective screening length and the film thickness. It will tend to zero for thick films ($m \rightarrow \infty$) but can become sizable when the film thickness becomes comparable to λ_{eff} . The ratio between the residual field into the ferroelectric (Eq. 7) and the bare depolarizing field quantifies the quality of the screening and can be expressed as $1 - \beta = 2\lambda_{eff}/ma_0$ (as it will be further discussed in Sec. III-C).

The depolarizing field can be computed averaging^{73,74,75} the microscopic electrostatic potential provided by a first-principles calculation for the whole capacitor. Details on the methodology and practical recipes to perform this nano-smoothing can be found in Ref. 76. Since the atomic positions, and therefore the induced polarization [Eq. (2)], and the thickness of the film are input variables of the simulation, λ_{eff} can be estimated using Eq. (7) once \mathcal{E}_d is known.

Junquera and Ghosez reported a value of $\lambda_{eff} = 0.23 \text{ \AA}$ (one order of magnitude smaller than the interplanar distances in the heterostructure) for their frozen phonon calculations on a $\text{SrRuO}_3/\text{BaTiO}_3/\text{SrRuO}_3$ capacitor. It might be even slightly smaller when the atomic relaxation of the metal is properly treated.⁷⁷ It is worth noticing that the effective screening length introduced in this model is NOT an intrinsic property of the metal (like the Thomas-Fermi screening length), but a quantity that strongly depends also on the details of the ferroelectric/electrode interface such as the different chemical bonds formed at the junction, or the penetration of electronic wave functions of the metal into the ferroelectric and vice versa. As shown by Sai *et al.*,⁷⁸ λ_{eff} can vary and become very small for some specific metal/ferroelectric interfaces. Understanding and controlling this compensation mechanism of the polarization charges in order to stabilize a uniform switchable polarization in the film is one of the challenges in the field of thin film ferroelectrics.⁵

Other authors^{79,80} alternatively explain the origin of a residual depolarizing field inside the ferroelectric thin film from the presence of a “dead layer” at the metal/ferroelectric interface. Although evoking a different mechanism, the theory of the dead layer yields very similar mathematical expressions than the theory of the imperfect metal screening discussed above, the role of the effective screening length being played by the thickness of the dead layer (see for instance Ref. 2, or compare the formulas of Ref. 81 by Bratkovsky and Levanyuk with those of Ref. 82 by Chensky and Tarasenko). Stengel and Spaldin⁸³ recently

reconciled these two apparently antagonist theories, providing a unified interpretation. Using a first-principles approach, they showed that the origin of an intrinsic dead layer with poor dielectric properties at the interface in oxide nanocapacitors is related to the hardening of the collective zone center polar modes that itself is produced by the incomplete screening of the depolarizing field.

In the presence of a non-vanishing electric field, the proper energy to be considered and minimized is no more the internal energy $U(\xi)$ of the crystal but a field-dependent energy potential $F(\xi, \mathcal{E})$ that, on top of $U(\xi)$, also includes an electrostatic energy term arising from the coupling between the polarization and the field.⁸⁴ This coupling term is proportional to $-\mathcal{E}_d \cdot P$. Since the depolarizing field is proportional to $(-P)$ [Eq. (7)] the additional electrostatic term in F is proportional to P^2 and positive in sign. Remembering Eq. (2), we see that proper treatment of the electrostatic energy will produce an additional term in Eq. (4) of the form $+\alpha\xi^2$. So, it clearly appears that, in a way similar to the epitaxial strain in Sec. III A, the incomplete screening of the depolarizing field is responsible for a renormalization of the quadratic coefficient of the energy. In this case however, the correction term is always positive ($\alpha \geq 0$) and therefore its effect contributes to suppress ferroelectricity.

The depolarizing field is inversely proportional to the thickness of the ferroelectric layer, Eq. (7). The thinner the film, the larger the depolarizing field and the larger the energy penalty to stabilize a monodomain pattern of the polarization. In order to minimize the energy while remaining in a homogeneous configuration, the ferroelectric suffers a progressive reduction of the polarization that show itself well above the critical thickness. This point was first confirmed experimentally by Lichtensteiger *et al.*⁸⁵ for PbTiO_3 monodomain epitaxial films through X-ray diffraction (XRD) measurement of the evolution of tetragonality c/a with thickness. The tetragonality indeed provides indirect but easily accessible information on the polarization through the polarization-strain coupling [from Eq. (3), $(c/a)_P = (c/a)_0 + \gamma P^2$] so that its measurement has become a standard technique to investigate size effects in thin films and superlattices.^{85,86,87} The reduction of the polarization was further confirmed by polarization data of Kim *et al.*⁸⁸ in ultrathin $\text{SrRuO}_3/\text{BaTiO}_3/\text{SrRuO}_3$ capacitors free from passive layers,⁸⁹ and more recent X-ray photoelectron diffraction (XPD) experiments of Despont *et al.*⁹⁰

As it was mentioned before, an alternative way of reducing the electrostatic energy is the

formation of 180° domains. In other words, going below the critical thickness predicted for monodomain configuration in ferroelectrics does not necessarily imply a paraelectric state.⁹ The existence of 180° domains prevent the appearance of a *net* interfacial charge density.⁹¹ This situation is well known in ferroelectric films on insulating substrates, where alternating 180° stripe domains structures have been observed and characterized analyzing the satellite peaks in synchrotron X-ray diffraction measurements.^{63,64} Even on conducting substrates, where the free charges of the electrode should provide a substantial amount of screening, the formation of 180° domains has been proposed to explain concomitant suppression of polarization and recovery of full tetragonality in $\text{Pb}(\text{Zr}_{0.2}\text{Ti}_{0.8})\text{O}_3$ on SrRuO_3 .⁹² This is supported with recent works based on the Landau theory,⁹³ that conclude that domains always form in thin films, almost irrespective of the nature of the electrode and whether or not the screening carriers may be present in the ferroelectric itself.

The situation is more complex experimentally, and whether the system breaks up into domains or not seems to be a very subtle issue. Lichtensteiger *et al.*, using the same experimental setup, have observed how high-quality ultrathin films of PbTiO_3 grown on Nb-SrTiO_3 electrodes remain in a monodomain configuration⁸⁵ (although with reduced polarization and tetragonality) whereas they form domains when the electrode is replaced by $\text{La}_{0.67}\text{Sr}_{0.33}\text{MnO}_3/\text{SrTiO}_3$.⁹⁴ Even in the case of insulating substrates, the formation of domains depends on how quickly the sample is cooled. Monodomain phases of PbTiO_3 on insulating SrTiO_3 have been grown and the structure have been analyzed with a coherent Bragg rod analysis (COBRA) method,⁹⁵ when the samples were cooled from deposition temperature to room temperature over a period of 24 hours, in contrast to the 180° stripe periods observed before.^{63,64} Nevertheless, even in the latter case, the system can no more be properly called ferroelectric since, although locally polarized, its polarization is no more expected to be switchable.⁹²

C. First-principles modeling of ferroelectric capacitors considering mechanical and electrical boundary conditions.

From the previous discussion, it is clear that appropriate treatments of the strain and of the incomplete screening of \mathcal{E}_d are crucial to describe size evolution of the ferroelectric properties. Very recently, many DFT calculations as well as first-principles-based effective

Hamiltonian or atomistic shell-models simulations have been reported addressing the problem of the thickness dependence of the ferroelectric properties in thin films, and the eventual existence of a critical thickness for ferroelectricity.

A summary of various results obtained with DFT based methods is reported in Table-I. In almost all these simulations, the prototype ferroelectric capacitor considered is made of an insulating layer of a ferroelectric perovskite oxide material (typically BaTiO_3 , PbTiO_3 or KNbO_3) sandwiched between metallic electrodes (typically a conductive oxide such as SrRuO_3 or a noble metal such as Pt), although lately a free top surface and some adsorbed molecules have been also simulated.^{60,61} Typically the capacitor is built with two symmetric metal-ferroelectric interfaces, although very recently Gerra and coworkers¹¹⁰ have explored asymmetric heterostructures and linked the first-principles computations with phenomenological approaches. The calculations were performed under short-circuit electrical boundary conditions for the electrodes (zero bias), a requirement that can be satisfied both in a ferroelectric/metal superlattice geometry or in a periodic metal/ferroelectric/metal/vacuum geometry^{112,113} (it is only recently that a method has been proposed to address finite bias with periodic boundary conditions¹¹¹). In all the previous approaches, a monodomain configuration was considered, so the electrode was the only source of screening of the polarization charge. The mechanical boundary-conditions were imposed by fixing the in-plane lattice constant and geometry to the one imposed by the substrate. The final constraint depends on the author, but the most common approach was to assume a strain imposed by SrTiO_3 , the typical substrate on top of which these capacitors are epitaxially grown. The minimum of the Kohn-Sham energies were then searched either by a frozen-phonon method within the ferroelectric soft mode subspace (line minimization displacing the atoms in the ferroelectric layer by hand with an amplitude corresponding to a given percentage of the bulk soft mode as defined in Sec. II) or by a full atomic relaxation of the atomic positions within the whole system. The results are summarized in Table-I and deserve two important comments.

First, although an exhaustive comparison of the results would certainly require to consider also other differences in the calculations, it is observed that DFT calculations performed within the Generalized Gradient Approximation (GGA) systematically overestimate the ferroelectric character compared to those within the local density approximation (LDA): while LDA predicts the existence of a critical thickness for ferroelectricity that ranges between two and six unit cells (depending on the material, electrode, interface, and strain condi-

TABLE I: Review of the most recent fully first-principles simulations on the ferroelectric properties of ferroelectric ultrathin films in a monodomain configuration. Both computations within the local density approximation (LDA) and the generalized gradient approximation (GGA) to the density functional theory have been reported in the literature. CA functional refers to Ceperley-Alder⁹⁶ in the parametrization of Perdew-Zunger,⁹⁷ while PW91 and PBE stand for the GGA functionals of Perdew and Wang^{98,99} and Perdew, Burke and Ernzerhof^{100,101} respectively. Regarding the method, NAO stands for numerical atomic orbitals as implemented in the SIESTA code,¹⁰² PW is the acronym for plane waves (as implemented in VASP^{103,104} in Refs. 77,105, or DACAPO¹⁰⁶ in Refs. 60,78), and MBPP stands for mixed-basis pseudopotentials.¹⁰⁷ a_{\parallel} represents the in-plane lattice constant. If a theoretical in-plane lattice constant is used to fix the length of the in-plane lattice vectors of the heterostructure, it is computed within the same method and approximations than in the simulation of the whole heterostructure. Different methodologies yield to slightly different values of the lattice constant. t_c stands for the critical thickness (if any) of the perovskite ultrathin film, in units of the number of cells of the ferroelectric perovskite oxide.

Reference	Heterostructure	Method	Functional	Interface	a_{\parallel}	t_c
Junquera <i>et al.</i> [70]	SrRuO ₃ /BaTiO ₃ /SrRuO ₃	NAO	LDA (CA)	SrO-TiO ₂	3.874 Å ($a_{\text{SrTiO}_3}^{\text{th}}$)	6
Junquera <i>et al.</i>	SrRuO ₃ /PbTiO ₃ /SrRuO ₃	NAO	LDA (CA)	SrO-TiO ₂	3.874 Å ($a_{\text{SrTiO}_3}^{\text{th}}$)	6
Gerra <i>et al.</i> [77]	SrRuO ₃ /BaTiO ₃ /SrRuO ₃	PW	GGA (PW91)	SrO-TiO ₂	3.94 Å ($a_{\text{SrTiO}_3}^{\text{th}}$)	3
Umeno <i>et al.</i> [108]	Pt/PbTiO ₃ /Pt	MBPP	LDA (CA)	Pt-PbO	3.845 Å ($a_{\text{SrTiO}_3}^{\text{th}}$)	4
				Pt-TiO ₂		6
				Pt-PbO	3.905 Å ($a_{\text{PbTiO}_3}^{\text{exp}}$)	No
			GGA (PW91)	Pt-TiO ₂		No
				SrO-NbO ₂	3.905 Å ($a_{\text{SrTiO}_3}^{\text{exp}}$)	4
				Pt-NbO ₂		2
Duan <i>et al.</i> [105]	SrRuO ₃ /KNbO ₃ /SrRuO ₃	PW	LDA (CA)	SrO-TiO ₂	3.991 Å ($a_{\text{BaTiO}_3}^{\text{exp}}$)	> 4
Na Sai <i>et al.</i> [78,109]	Pt/BaTiO ₃ /Pt	PW	GGA	RuO ₂ -BaO		> 4
				Pt-TiO ₂		> 4
				Pt-BaO		> 4
				SrO-TiO ₂	3.905 Å ($a_{\text{PbTiO}_3}^{\text{exp}}$)	No
				RuO ₂ -PbO		No
	SrRuO ₃ /PbTiO ₃ /SrRuO ₃	PW	GGA	Pt-TiO ₂		No
				Pt-PbO		No
				SrO-TiO ₂	$a_{\text{PbTiO}_3}^{\text{th}}$	> 3
				SrRuO ₃ /PbTiO ₃ /OH, O or H		< 3
				SrRuO ₃ /PbTiO ₃ /CO ₂		~ 3
D. D. Fong <i>et al.</i> [60]	SrRuO ₃ /PbTiO ₃ /H ₂ O	PW	GGA	SrO-TiO ₂		> 3

tions), calculations within the GGA often result in the absence of such a limit, especially in Pb-based perovskites, with ferroelectric ground states that are stable down to the ultimate thickness of one unit cell, eventually with an enhancement of the polarization.^{78,108} To interpret this trend it is worth to notice that, although GGA might a priori be considered as an improvement over LDA, it does not necessarily produce more trustable results in the case of ferroelectric oxides. At the bulk level, the widely used GGA of Perdew, Burke and Ernzerhof (GGA- PBE)¹⁰⁰ has been shown to strongly overestimate the ferroelectric character and, even, to yield an erroneous super-tetragonal structure in PbTiO_3 ^{108,114,115} and BaTiO_3 .¹¹⁵ Only the recently proposed improved GGA functional of Wu and Cohen¹¹⁶ solves this problem and produces very accurate structures. The GGA results of Table-I are not making use of this new functional so that their comparison with LDA results must be made with caution : indeed, the fact that GGA overestimates the ferroelectric character and concludes sometimes in the absence of critical thickness might be, at least partly, an artifact similar to that reported at the bulk level.

Second, it is well-known that the bandgap of the Kohn-Sham particles as computed within DFT is significantly smaller than the experimental gap. For BaTiO_3 , typical LDA values are of the order of 1.6–1.9 eV^{115,117} while the experimental value is of 3.2 eV. Although this DFT bandgap problem does not a priori constitute a failure of the theory that should internally correct for it, at least in “exact” DFT, in order to provide correct ground-state properties, it can yield unphysical results when working with approximate functionals. The band alignment at a typical metal/ferroelectric interface is illustrated in Fig. 4a where, for the purpose of the illustration, the Fermi level of the metal is assumed to be located roughly mid-gap, as typically expected from the experiment. The DFT bandgap underestimate prevents accurate predictions of the barriers simultaneously for electrons, ϕ_n , and holes, ϕ_p , and can in many cases produce pathological situations where the Fermi level of the metal is erroneously aligned with the conduction bands of the ferroelectric ($\phi_n < 0$), producing unphysical population of the conduction bands of the ferroelectric (Fig. 4c). Such a situation was, for instance, reported by the authors of Ref. 83 for the Pt/ SrTiO_3 interface, the structure of which had to be artificially modified to avoid the problem, or also appears from the analysis of the partial density of states of the Pt/ BaTiO_3 interface in Ref. 118. Moreover, even in “normal” cases where the DFT calculation reproduces a small barrier for electrons in a non-polarized configuration (Fig. 4b), the situation remains problematic

since the underestimate of the electron barrier artificially lowers the breakdown field: if during the relaxation of the ferroelectric state, the residual depolarizing field exceeds the erroneously low DFT breakdown field, a spurious transfer of electrons from the metal to the ferroelectric conduction bands will be observed at the interface, modifying its properties and producing an unphysical relaxed structure. For the SrRuO₃/BaTiO₃/SrRuO₃ nanocapacitor of Ref. 70, we obtained within the LDA for the non-polar configuration $\phi_p^{LDA} = 1.47$ eV and $\phi_n^{LDA} = 0.11$ eV, while the use of an empirical “scissors” correction (i.e. a rigid shift in energy of the BaTiO₃ conduction bands of 1.62 eV, to reproduce the experimental bandgap) provides a more realistic value $\phi_n^{SCI} = 1.73$ eV.¹¹⁷ The artificially low value of ϕ_n^{LDA} prevented us to perform full atomic relaxations of the ferroelectric state but was not addressed by other authors reporting full relaxation on the same system.

All these issues highlight that special care must be taken when dealing with metal/ferroelectric interfaces and invite to be specially critical when interpreting the results. An important challenge at this point for the theoreticians is to identify an alternative functional avoiding the bandgap problem and its consequences on the band alignment, while preserving accurate description of the structural and ferroelectric properties. The B1 hybrid functional recently proposed by Bilc *et al.*¹¹⁵ might constitute an promising option.

In spite of the technical difficulties highlighted above, first-principles DFT simulations remain the most accurate model currently available for the theoretical study of ferroelectric capacitors and provides a wealth of informations at the atomic level. Calculations are however performed at 0 K, so that the study of the temperature dependence of the structural, ferroelectric, and piezoelectric properties is not accessible. Also, DFT calculations are computationally very demanding and the effort required to deal with such complex heterostructures, involving interfaces between dissimilar metal/insulator materials, is at the limit of present capabilities. To bypass these intrinsic limitations and address more complex questions, alternative less accurate methods have been proposed that remain based on first-principles results. These include effective Hamiltonian,^{34,46} shell model,^{119,120,121} and molecular dynamics simulations combined with coarse-grained Monte Carlo simulations,¹²² where the different parameters are directly fitted on DFT results.

Wu and coworkers^{123,124} have performed effective Hamiltonian simulations on Pb(Zr_{0.5}Ti_{0.5})O₃ free standing slabs. The choice of the Ti and Zr composition is interesting, since it is close to the morphotropic phase boundary of bulk PZT. Since the calculations

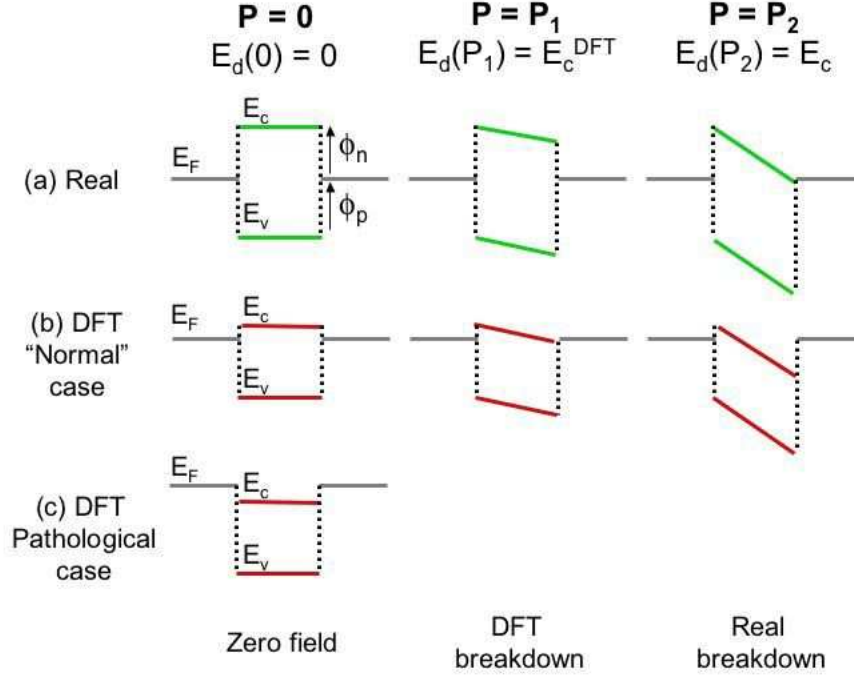


FIG. 4: Schematic band alignment in a typical metal/ferroelectric/metal capacitor. In the paraelectric state, due to the DFT bandgap problem, the Schottky barrier ϕ_n is underestimated (b), and can eventually produce pathological situations where $\phi_n < 0$ (c). In the ferroelectric state ($P \neq 0$), the DFT bandgap problem will additionally be responsible for a lowering of the breakdown field \mathcal{E}_c to $\mathcal{E}_c^{\text{DFT}}$. If the residual depolarizing field \mathcal{E}_d associated to the ground-state polarization exceeds $\mathcal{E}_c^{\text{DFT}}$, a spurious transfer of electrons from the metal to the ferroelectric conduction bands will be observed at the interface and produce unphysical results.

were done in the absence of surface charge screening, films thicker than 4 unit cell form 180° domains in the direction normal to the surface to screen the depolarizing field, so the average component of the out-of-plane local mode vanishes, independently of the strain. The depolarizing field does not influence the in-plane polarization versus strain behaviour. A rich strain-temperature phase diagram, including a monoclinic and a stripe domain phase not present in the bulk parent material was predicted.

For the same composition of $\text{Pb}(\text{Zr}_{0.5}\text{Ti}_{0.5})\text{O}_3$, Kornev *et al.*¹²⁵ extended the effective Hamiltonian in order to incorporate explicitly the presence of a free surface and the effects of a partial compensation of the depolarizing field. As in Ref. 92, in this first attempt, only the net component of the out-of-plane polarization at the surface layers was considered

to compute the homogeneous depolarizing field and the corresponding contributions to the energy. The treatment of \mathcal{E}_d was then refined by Ponomareva and coworkers,¹²⁶ who corrected the dipole-dipole interactions of the bulk model hamiltonian by summing explicitly contributions of the local dipoles present within the film, and derived in this way an *exact* expression for the depolarizing energy and field at an atomistic level in any low dimensional ferroelectric structure under open circuit (OC) boundary conditions. If the polarization lies along a non-periodic direction, the OC boundary conditions naturally lead to the existence of a maximum of the depolarizing field that is later screened by hand. The amount of screening and therefore the amplitude of the residual field can be tuned with a parameter, β (see Section III-B), that plays a role similar to the effective screening length in the model described above and ranges between $\beta = 0$ (OC boundary conditions) and $\beta = 1$ (perfect short circuit boundary conditions). This model has been applied to different kinds of low dimensional ferroelectrics.¹²⁷

In Ref. 125, the interplay between the screening of the depolarizing field and the strain imposed by the substrate was also explored. In the limit of perfect screening, a uniform polarization along z is predicted, while the behaviour of the in-plane components of the polarization depends on the strain, following the general rule described in Sec. III A: a compressive strain suppresses the in-plane polarization while a tensile strain favours the presence of a *aa*-phase. Therefore, the phase change from a monoclinic phase (the so-called M_A phase with $\langle P_x \rangle = \langle P_y \rangle \neq 0$, $\langle P_z \rangle > \langle P_x \rangle$) for sufficiently large tensile strains to a tetragonal phase with $\langle P_x \rangle = \langle P_y \rangle = 0$, $\langle P_z \rangle > 0$ for stress free or compressive strains. On the other extreme case of open-circuit boundary conditions, the *average* polarization along z vanishes independently of strain, while the in-plane polarization aligns with the $[010]$ direction ($\langle P_y \rangle \neq 0$, $\langle P_x \rangle = 0$) for the stress free, displays a monoclinic M_c phase ($\langle P_x \rangle \neq \langle P_y \rangle \neq 0$, $\langle P_y \rangle > \langle P_x \rangle$) under tensile strain, or vanishes for compressive strain. For intermediate values of the depolarizing field, the polarization continuously rotates and passes through low-symmetry phases. Interestingly, these phases are stable only for compositions lying near the morphotropic phase boundary of bulk PZT, disappearing in favour of a tetragonal phase for high enough Ti-concentrations. The fact that the *average* out-of-plane polarization vanishes under open circuit boundary conditions does not mean that the local dipoles along z vanishes. On the contrary, they might have a large value, close to the bulk one, but forming domains. The process of formation of these domains was monitored with

respect the screening of the depolarizing field. When \mathcal{E}_d is large enough, some “bubbles” (cylindric nanodomains having local dipoles that are aligned in an opposite direction with respect the one in the monodomain configuration) nucleate and grow laterally till 180° stripe domains are formed.

Model hamiltonian techniques have the additional advantage of a trivial treatment of external electric fields. Starting from a five unit cell thick thin film geometry under compressive strain, where c -oriented 180° stripe domains are stabilized even assuming a realistic amount of screening of the depolarizing field, the evolution of the domain structure under an electric field has been studied for $\text{Pb}(\text{Zr}_{0.5}\text{Ti}_{0.5})\text{O}_3$ ¹²⁸ and BaTiO_3 ,¹²⁹ giving some light into the mechanisms to saturate the films. The path is essentially the same for both perovskites oxides and consist of three different steps: (i) the growth of the domain parallel to the field at the expense of the other up to a first threshold value of the external field; (ii) the formation of the nanobubbles defined before; and (iii) the contraction of the nanobubbles till the final collapse into a monodomain configuration at a second critical value of the external field. The main differences between BaTiO_3 and $\text{Pb}(\text{Zr}_{0.5}\text{Ti}_{0.5})\text{O}_3$ are (i) the orientation of the domain walls: the stripes alternate along [110] for BaTiO_3 rather than along [100] for $\text{Pb}(\text{Zr}_{0.5}\text{Ti}_{0.5})\text{O}_3$, and (ii) the “hardness” of the polarizarion in BaTiO_3 to rotate (BaTiO_3 films profoundly dislike significantly rotating and in-plane dipoles).

The formation and response of the “bubbles” to external electric fields and the recent predictions of domains of closure^{130,131,132} (very common in ferromagnets but detected in ferroelectric thin films only recently¹³³), have bridged a fascinating parallelism between ferroelectric and ferromagnetic domains. Although the shape and size of the “bubbles” (elliptical in ferroelectrics and spherical in ferromagnets), the abruptness of the domain walls (one lattice constant thick in ferroelectrics and much more gradual, over many atomic planes, in ferromagnets), or the exceptionally small periodicity and constancy with the field of the ferroelectric domain periods differ from the counterpart ferromagnetic properties, they might not be so different as traditionally considered, despite the profound differences between electrostatic and magnetostatic interactions. Domains of closure have been predicted using a first-principles effective hamiltonian for $\text{Pb}(\text{Zr}_{0.4}\text{Ti}_{0.6})\text{O}_3$ ¹³⁴ asymmetrically screened (grown on a nonconducting substrate and with a metal with a dead layer as top electrode), and using a Landau-Ginzburg phenomenological approach for a PbTiO_3 thin film,¹³⁵ both asymmetrically and symmetrically coated with insulating SrTiO_3 . These predictions have obtained

further credit after full first-principles simulations on $\text{SrRuO}_3/\text{BaTiO}_3/\text{SrRuO}_3$ ferroelectric capacitors by Aguado-Puente and Junquera,¹³⁶ where the domains of closure are obtained even for a symmetrical metal/ferroelectric/metal capacitor, where the metallic plates should provide significant screening. As it happens with ferromagnetic domains, ferroelectric domains follow the Kittel law (that states that the domain width is directly proportional to the square root of the sample's thickness), at least for thicknesses thicker than 1.2 nm.¹³⁷

The effective Hamiltonian approach is now considered as a standard method and has been used to address various other questions. The phase diagram of PZT films as a function of temperature and Ti composition under open-circuit boundary conditions has been reported in Ref. 138. Other systems like BaTiO_3 have also been considered for which the strain/temperature phase diagram has been obtained and the effect of incomplete screening of \mathcal{E}_d has been discussed.⁵¹ Although most studies focused on [001] epitaxial films, the influence of the growth direction on the properties was also investigated.¹³⁹

Besides all the previous theoretical frameworks, molecular dynamics combined with coarse-grained Monte Carlo simulations have been recently used to study a very important technological problem: the switching of the ferroelectric polarization.¹²² These simulations show that the shape of the critical nucleus is square and not a thin triangular plate as suggested by the prevailing Miller-Weinrich model. The critical nuclei grow in an anisotropic way, with activation barriers for sideways and forward growth much smaller than for nucleation. The values for the activation energies and activation fields predicted by the molecular dynamics simulations are one order of magnitude smaller than those expected from the Miller-Weinrich theory, mainly due to the new slanted interface model for the surface of the nuclei, and the domain velocities are in very good agreement with the ones measured experimentally.¹⁴⁰

IV. SUPERLATTICES

Artificial ferroelectric superlattices are nowadays considered as an interesting alternative to ferroelectric thin films¹⁴¹ since, as it is discussed below, they allow fine tuning of the ferroelectric properties while maintaining perfect crystal ordering. The large variety of materials that can be combined (ferroelectrics, incipient ferroelectrics or regular insulators) and the way these materials can be ordered within the structure (bicolor and tricolor superlattices

or even more complex structures with composition gradients) also offers tremendous scope for creating artificial ferroelectric materials with possibly new and tailor-made properties.

During the recent years, short-period epitaxial multilayers combining a ferroelectric and an incipient ferroelectric material (like $\text{BaTiO}_3/\text{SrTiO}_3$,^{41,42,142,143,144,145,146,147,148,149,150,151,152,153} $\text{PbTiO}_3/\text{SrTiO}_3$,^{86,87,154,155} $\text{KNbO}_3/\text{KTaO}_3$,^{156,157,158,159} and related tricolor systems like $\text{BaTiO}_3/\text{SrTiO}_3/\text{CaTiO}_3$ ^{160,161,162}) have retained most of the attention both at the theoretical and experimental level. In these systems, proper handling of the mechanical and electrical boundary conditions appears crucial to monitor the ferroelectric properties in a way very similar to what was previously discussed for thin films.

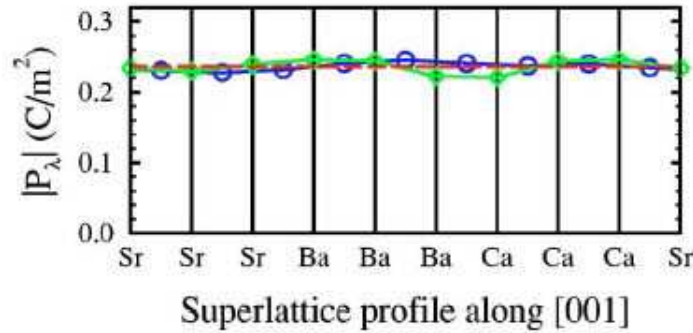


FIG. 5: Layer by layer polarization profile along a ferroelectric $\text{BaTiO}_3/\text{SrTiO}_3/\text{CaTiO}_3$ multilayer as obtained from DFT first-principles calculations. A polarization similar to that of BaTiO_3 is induced in the non-ferroelectric SrTiO_3 and CaTiO_3 layers. Figure taken from Ref. 161.

First, the alternation of ultrathin layers is particularly suited to impose coherent epitaxial strains and achieve “strain engineering” of the properties. The compressive epitaxial strain produced by a SrTiO_3 substrate on BaTiO_3 layers contributes to explain polarization enhancement with respect to the bulk BaTiO_3 value in $\text{BaTiO}_3/\text{SrTiO}_3$ bicolor superlattices^{41,42,152} and even in tricolor¹⁶⁰ superlattices, despite the fact that part of the system is not nominally ferroelectric. The epitaxial strain additionally produces significant shift of the phase transition temperature as for instance reported for $\text{BaTiO}_3/\text{SrTiO}_3$ ¹⁵² and $\text{PbTiO}_3/\text{SrTiO}_3$ ⁸⁷ superlattices. Ferroelectricity is even expected in $\text{SrZrO}_3/\text{SrTiO}_3$ superlattices on SrTiO_3 , in spite of the fact that neither SrZrO_3 nor SrTiO_3 is ferroelectric at the bulk level.¹⁶³ Although it was not stated by the authors, this can probably be partly explained from the large compressive strain imposed on the SrZrO_3 layers by the SrTiO_3

substrate.

Second, electrostatic coupling between the layers is also playing a key role. On the one hand, polarizing the ferroelectric BaTiO_3 layers only in a $\text{BaTiO}_3/\text{SrTiO}_3$ superlattice would produce a large polarization gradient at the interfaces, inducing huge depolarizing fields and electrostatic energy. On the other hand, polarizing SrTiO_3 also has an energy cost since this material is not spontaneously polarized. The ground-state of the system will therefore depend on the competition between different energy terms and can strongly evolve depending of the compounds involved and the superlattice period.

In short-period superlattices where the ferroelectric alternates with a highly polarizable compound such as an incipient ferroelectric (like SrTiO_3 or KTaO_3), a polarization will be induced in the latter in order to avoid depolarizing fields and the superlattice will typically exhibit a homogeneously polarized configuration (see Fig. 5). First pointed out by Neaton and Rabe on $\text{BaTiO}_3/\text{SrTiO}_3$ superlattices, such a behavior was also theoretically predicted for $\text{PbTiO}_3/\text{SrTiO}_3$,⁸⁶ or even $\text{BaTiO}_3/\text{SrTiO}_3/\text{CaTiO}_3$ ^{161,162} short-period superlattices. In many theoretical studies, the layer polarization was estimated roughly, multiplying the atomic displacements into the layer by the bulk Born effective charges. A more rigorous and accurate approach has been proposed recently based on Wannier functions.¹⁶⁴

In a recent work, Dawber *et al.*⁸⁷ have demonstrated that key ferroelectric properties can be tuned over a very wide range in $\text{PbTiO}_3/\text{SrTiO}_3$ superlattices: it was shown that the polarization can be adjusted from 0 to $60 \mu\text{C}/\text{cm}^2$ and the transition temperature from room temperature to 700°C by properly adjusting the volume fraction of PbTiO_3 . Moreover, a simple Landau-based model was proposed that allows to determine a priori the properties of the system, so opening the way to the production of samples with ferroelectric properties designed for particular applications. It was also reported that the presence of SrTiO_3 between the PbTiO_3 layers in the superlattice improve the electrical properties and allows to avoid the large leakage currents typically reported in PbTiO_3 thin films while maintaining perfect crystal structure.

The simple arguments described above have been shown to provide reasonable description of $(\text{PbTiO}_3)_n/(\text{SrTiO}_3)_3$ superlattices over a relatively wide range of PbTiO_3 thicknesses (for n ranging from 1 to 53).⁸⁶ They are however expected to apply mainly to relatively short-period systems. In longer period superlattices, other behaviors are expected. In $\text{KNbO}_3/\text{KTaO}_3$ ¹⁵⁷ it was theoretically shown using a shell-model that the electrostatic

coupling between layers (responsible for a homogeneous polarization throughout the system) will progressively decrease as the period increases, yielding a progressive reduction of KTaO_3 polarization. In $\text{BaTiO}_3/\text{SrTiO}_3$,¹⁵³ effective Hamiltonian simulations have confirmed that short-period superlattices behave like a homogeneous-like material with a phase diagram that resembles that of a (001) BaTiO_3 thin film under short-circuit conditions while inhomogeneous atomic features and original domain patterns were predicted in longer period systems. Appearance of domain structures in ferroelectric/paraelectric superlattices was also discussed by Stephanovich *et al.*¹⁶⁵

The previous discussion implicitly focused on the evolution of the out-of-plane polarization. In some cases, an in-plane component of the polarization can also eventually appear. This was predicted in $\text{KNbO}_3/\text{KTaO}_3$ superlattices in which the epitaxial compressive strain is not strong enough to force KNbO_3 (with a rhombohedral ground-state) to become tetragonal.¹⁵⁹ In a way compatible with a symmetry lowering observed experimentally,¹⁴⁹ an in-plane polarization component was also predicted in the SrTiO_3 layers of $\text{BaTiO}_3/\text{SrTiO}_3$ superlattices under in-plane expansion.¹⁵⁰ The main difference between the out-of-plane and in-plane polarization components is that while the out-of-plane components of the different layers are strongly electrostatically coupled as previously discussed, the in-plane components behaves much more independently and remain confined in the individual layers in which they are induced by the epitaxial strain conditions imposed by the substrate.

The interest for ferroelectric superlattices is not limited to the fact that they allow the tuning of the ferroelectric properties as discussed above but also results from their potentiality to generate totally new behaviors or phenomena. In $\text{Pb}(\text{Sc}_{0.5+x}\text{Nb}_{0.5-x})\text{O}_3$ (PSN)¹⁶⁶ and $\text{Pb}(\text{Zr}_{1-x}\text{Ti}_x)\text{O}_3$ (PZT)¹⁶⁷ superlattices, it is expected that symmetry lowering can yield new stable polar phases and strong enhancement of the functional properties. Unusual thermoelectric properties and nonergodicity were also predicted in PZT superlattices.¹⁶⁸ In very short-period $\text{PbTiO}_3/\text{SrTiO}_3$ superlattices an unexpected recovery of ferroelectricity has been observed in the limit of ultrathin PbTiO_3 layers that cannot be explained from the simple arguments reported above.^{86,87,155} Beyond such bicolor systems, tricolor superlattices, which break the inversion symmetry¹⁶⁹ are also expected to potentially exhibit unusual and attractive properties.

First-principles based simulations contributed to make significant progresses in the understanding of the behavior of ferroelectric superlattices and even opened the door to a

possible theoretical design of artificial ferroelectric nanostructures with predetermined and tailor-made properties.¹⁷⁰

V. NANOPARTICLES AND NANOWIRES

Although most of the recent experimental and theoretical efforts on ferroelectric nanostructures concerned thin films geometries, the growth and characterization of ferroelectric nanowires,^{171,172} nanotubes,^{173,174} nanocolumns,¹⁷⁵ nanoislands,¹⁷⁶ or even “nanosolenoids”¹⁷⁷ are at an incipient and exciting state. The geometries of these nanostructures favor novel inhomogeneous polarization and strain configurations, strongly dependent of the electrical and mechanical boundary conditions.

DFT first-principles studies of such low dimensional structures are, however, computationally very demanding. Other recent studies made use of first-principles based shell-models¹²¹ and model hamiltonian methods.¹⁷⁸ For instance, domain structures, polarization and coercive fields of nanoscopic particles of BaTiO₃ have been carried out using such methodologies.

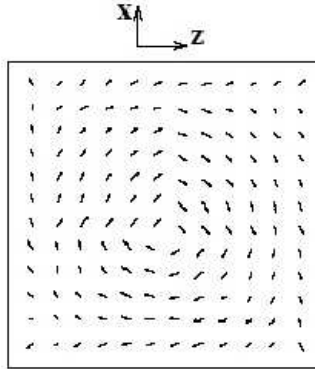


FIG. 6: “Vortex-like” structure of the local polarization in a $(12 \times 12 \times 12)$ BaTiO₃ quantum dot. The figure corresponds to a cut along the $y = 6^{th}$ plane. Although the macroscopic polarization vanishes the toroid moment of the vortex structure has a well-defined finite value. Figure taken from Ref. 178.

Perhaps, the most remarkable result is the prediction of novel exotic geometric ordering of ferroelectricity in BaTiO₃¹⁷⁸ and Pb(Zr_{0.5}Ti_{0.5})O₃^{179,180} nanoscale disks and rods, where the local polarization rotate from cell to cell, forming a “vortex-like” pattern. Although the

macroscopic polarization of these quantum dots vanishes at zero applied field, they exhibit a new order parameter, the *toroid moment* of polarization, introduced by Naumov *et al.*¹⁷⁹ and defined as

$$\vec{G} = \frac{1}{2N} \sum_i \vec{R}_i \times \vec{p}_i, \quad (8)$$

where \vec{p}_i is the local dipole of cell i located at \vec{R}_i , and N is the number of unit cells in the simulation. Since the local dipoles in the vortex can rotate either clockwise or anticlockwise, the toroid moment might adopt two different values pointing in opposite directions, so that one bit of information might be stored by assigning one value of the Boolean algebra (“1” or “0”) to each of these states. The direction of the toroidal moment can be efficiently controlled by a transverse inhomogeneous electric field generated by two opposite charges located away from the studied dot,¹⁸¹ opening exciting opportunities for nanomemory devices. Technologically, the ferroelectric vortex phase promises to increase the storage density of ferroelectric random access memories (Fe-RAM) by five orders of magnitude.

In order to investigate the possibility of engineering the dipole patterns and vortex structures, a study of the phase diagram as a function of temperature of these ferroelectric nanodots when they are embedded in a polarizable medium was reported by Prosandeev and Bellaiche.¹⁸² Six different phases were found, depending on the ferroelectric strength of the material constituting the dot and of the system forming the medium. Some of the novel phases are remarkable, for instance the coexistence of a toroidal moment and a spontaneous polarization at low T when a soft ferroelectric dot is immersed in a medium that is ferroelectrically harder than the dot. Medium driven interactions between dots were demonstrated with adjacent vortices rotating in an opposite fashion (“antiferrotoroidic” phase).

The phase transition from the vortex structure (with the local dipoles circularly ordered) to a ferroelectric phase (with all the local dipoles pointing along the same direction and with an out-of-plane polarization) in a $\text{Pb}(\text{Zr}_{0.5}\text{Ti}_{0.5})\text{O}_3$ nanocylinder by an electric field perpendicular to the plane of the vortex has been recently addressed.¹⁸³ The transition between the two phases is through an intermediate state that generates a lateral toroid moment and breaks the macroscopic cylindrical symmetry. The observation of this new phase yielded to the discovery of a striking collective phenomenon, that leads to the annihilation of the ferroelectric vortex in a peculiar azimuthal mode.

A first step to explain the existence of this toroidal moment in ferroelectric nanoparticles from a DGL theory has been taken by Wang and Zhang¹⁸⁴ A more exhaustive review of all these computations can be found in Ref. 7.

In between the two-dimensional (2D) thin films and superlattices discussed in Secs. III and IV, and the zero-dimensional (0D) nanoparticles described above, the case of one-dimensional (1D) nanowires was also recently addressed. Model hamiltonian simulations on $\text{Pb}(\text{Zr,Ti})\text{O}_3$ ¹⁸⁵ and full first-principles simulations on BaTiO_3 nanowires¹⁸⁶ have demonstrated how long-range ordering exists in these 1D systems even at finite temperature and under zero external field. These results challenged traditional statistical models that claimed that 1D lattices with particle-particle interactions decaying faster than r^{-n} , $n \geq 3$, are impossible to have phase transitions at finite T. As it happened in thin films and nanoparticles, the mechanical and electrical boundary conditions are essential in the nanowires. The presence of uncoated free surfaces yields to the existence of depolarizing fields along two directions and forces the collective polarization to lie along the longitudinal direction. A critical diameter for the polarization was estimated around 1.2 nm for BaTiO_3 ¹⁸⁶ and 2.0 nm for $\text{Pb}(\text{Zr,Ti})\text{O}_3$,¹⁸⁵ below which the ferroelectricity was suppressed. At smaller radii, low atomic coordinations at the surface produce a contraction of the unit cell that is responsible for the suppression of the ferroelectric distortion at the critical radius. Nevertheless, even below this threshold size of the diameter, ferroelectricity might be recovered playing with the mechanical boundary conditions, by applying appropriate tensile strain.

Previous first-principles simulations on nanowires also contributed to get a new insight into the concept of the ferroelectric correlation volume, defined as the smallest volume within which atomic displacements must be correlated in order to decrease the energy of the crystal and produce a stable polar entity. Analyzing the critical diameter of the wire as a function of its length, the computations prove that is the anisotropic shape of the polar domain rather than its volume that determines the stability of its ferroelectric state.¹⁸⁷

VI. CONCLUSIONS AND PERSPECTIVES

As illustrated throughout this review, various progresses have been reported during the last years concerning the description of the ferroelectric properties in oxide ultrathin films and superlattices. In this context, first-principles theory and modeling constituted an ef-

ficient guide and provided a significant support to experimental works. On the one hand, proper understanding of the crucial role played by the electrical and mechanical allowed to realize significant advances as discussed above. On the other hand, however, many issues still remain unclear so that this field of research is still at an exciting and incipient stage.

In ferroelectric thin films, despite recent achievements, some important questions remain without clear answer and interesting perspectives ask for further confirmations. Only recently addressed from first-principles,⁶¹ the mechanism and the quality of the screening at free surfaces with air remains unclear. Also the reason why some ferroelectric films on metallic electrodes stay monodomain with a reduced polarization while others break into domains is particularly intriguing.⁹⁴ The roles of defects, such as oxygen vacancies, and of leakage currents on the amplitude of the depolarizing field was up to now neglected in theoretical studies while they might play a role, at least in some cases. The mechanism of the switching and domain-wall motion in ultrathin films is an important question that has been studied in detail experimentally^{140,188,189,190} but that has not been addressed yet at the first-principles level, although the first-steps on multi-scale computations based on molecular dynamics and coarse-grained Monte Carlo simulations have been recently taken.¹²² Recent studies reported interesting perspectives for ferroelectric tunnel junctions^{118,191,192} but no first-principles quantitative estimate of the tunneling current and of the electroresistance has been reported yet. Finally and without being exhaustive, the case of a ferroelectric layer between magnetic electrodes was proposed as a mechanism to achieve ferroelectric control of magnetism^{193,194} but is still widely unexplored.

Ferroelectric superlattices constitute a promising alternative avenue that offers practical solutions to bypass some of the drawbacks of epitaxial ultrathin films (huge depolarizing fields, high leakage currents, strain relaxation), while preserving perfect crystal ordering and allowing to monitor the ferroelectric properties. Up to now, fine tuning of the polarization and phase transition temperature has, for instance, been illustrated playing with the superlattice period and composition but the most exciting perspectives probably rely on the potentiality of such systems to generate totally new and unexpected phenomena. Also, superlattices might offer particularly attractive opportunities in the emergent field of magneto-electric multiferroics.¹⁹⁵

The perspectives are numerous and first-principles simulations will certainly continue to play an active role in the field of nanoscale ferroelectrics in the future. In some cases, this will

mandatory require new theoretical developments such as, for instance, the identification of alternative and more accurate functionals or of new efficient approaches to compute complex properties. In order cases, the computer power will constitute the main limitation. In all cases, pursuing the constructive dialog initiated during the recent years between theorists and experimentalists will certainly appear as a major motivation.

Acknowledgements

The authors thank J.-M. Triscone, M. Dawber, C. Lichtensteiger, H. Kohlstedt, M. Alexe, G. Geneste, E. Bousquet, and P. Aguado-Puente for valuable discussions. PhG acknowledges financial support from the VolkswagenStiftung (I/77 737), the Interuniversity Attraction Poles Program - Belgian State - Belgian Science policy (P6/42), the FAME European Network of Excellence and the MaCoMuFi European Strep project. JJ acknowledges financial support by the Spanish MEC under Project FIS2006-02261, and the Australian Research Council ARC Discovery Grant DP 0666231.

-
- ¹ C. H. Ahn, K. M. Rabe, and J.-M. Triscone, *Science* **303**, 488 (2004).
 - ² Ph. Ghosez and J. Junquera, First-Principles Modeling of Ferroelectric Oxide Nanostructures, in, *Handbook of theoretical and computational nanotechnology*, edited by M. Rieth and W. Schommers (American Scientific Publishers, Stevenson Ranch, CA, 2006), vol. 9, pp. 623–728.
 - ³ K. M. Rabe and Ph. Ghosez, First-Principles Studies of Ferroelectric Oxides, in *Physics of Ferroelectrics, a Modern Perspective* edited by K. M. Rabe, C. H. Ahn, and J.-M. Triscone (Topics of Applied Physics, Springer, Berlin, 2007), vol. 105, pp. 117–174.
 - ⁴ C. Lichtensteiger, M. Dawber, and J.-M. Triscone, Ferroelectric Size Effects, in *Physics of Ferroelectrics, a Modern Perspective* edited by K. M. Rabe, C. H. Ahn, and J.-M. Triscone (Topics of Applied Physics, Springer, Berlin, 2007), vol. 105, pp. 305–338.
 - ⁵ M. Dawber, K. M. Rabe, and J. F. Scott, *Rev. Mod. Phys.* **77**, 1083 (2005).
 - ⁶ K. M. Rabe, *Curr. Opin. Solid State Mat. Sci.* **9**, 122 (2005).
 - ⁷ I. Ponomareva, I. Naumov, I. Kornev, H. Fu, and L. Bellaiche, *Curr. Opin. Solid State Mat. Sci.* **9**, 114 (2005).

- ⁸ W. Duan and Z. R. Liu, Curr. Opin. Solid State Mat. Sci. **10**, 40 (2006).
- ⁹ J. F. Scott, J. Phys.: Condens. Matter **18**, R361 (2006).
- ¹⁰ N. Setter, D. Damjanovic, L. Eng, G. Fox, S. Gevorgian, S. Hong, A. Kingon, H. Kohlstedt, N. Y. Park, G. B. Stephenson, I. Stolitchnov, A. K. Taganstev, D. V. Taylor, T. Yamada, and S. K. Streiffer, J. Appl. Phys. **100**, 051606 (2006).
- ¹¹ M. E. Lines and A. M. Glass, *Principles and Applications of Ferroelectrics and Related Materials* (Clarendon Press, Oxford, 1977).
- ¹² A. F. Devonshire, Phil. Mag. **40**, 1040 (1949).
- ¹³ A. F. Devonshire, Phil. Mag. **42**, 1065 (1951).
- ¹⁴ W. Cochran, Adv. Phys. **9**, 387 (1960).
- ¹⁵ W. Zhong, R. D. King-Smith, and D. Vanderbilt, Phys. Rev. Lett. **72**, 3618 (1994).
- ¹⁶ M. Veithen and P. Ghosez, Phys. Rev. B **65**, 214302 (2002).
- ¹⁷ Ph. Ghosez, X. Gonze, and J.-P. Michenaud, Europhys. Lett. **33**, 713 (1996).
- ¹⁸ Ph. Ghosez, X. Gonze, and J.-P. Michenaud, Phys. Rev. B **58**, 6224 (1998).
- ¹⁹ R. E. Cohen, Nature **358**, 136 (1992).
- ²⁰ R. D. King-Smith and D. Vanderbilt, Phys. Rev. B **49**, 5828 (1994).
- ²¹ G. A. Samara, T. Sakudo, and K. Yoshimitsu, Phys. Rev. Lett. **35**, 1767 (1975).
- ²² I. A. Kornev, L. Bellaiche, P. Bouvier, P.-E. Janolin, B. Dkhil, and J. Kreisel, Phys. Rev. Lett. **95**, 196804 (2005).
- ²³ E. Bousquet and Ph. Ghosez, Phys. Rev. B **74**, 180101(R) (2006).
- ²⁴ A. Ruini, R. Resta, and S. Baroni, Phys. Rev. B **57**, 5742 (1998).
- ²⁵ L. Fu, E. Yaschenko, L. Resca, and R. Resta, Phys. Rev. B **60**, 2697 (1999).
- ²⁶ O. Diéguez, S. Tinte, A. Antons, C. Bungaro, J. B. Neaton, K. M. Rabe, and D. Vanderbilt, Phys. Rev. B **69**, 212101 (2004).
- ²⁷ A. V. Bune, V. M. Fridkin, S. Ducharme, L. M. Blinov, S. P. Palto, A. V. Sorokin, S. G. Yudin, and A. Zlatkin, Nature **391**, 874 (1998).
- ²⁸ Th. Tybell, C. H. Ahn, and J.-M. Triscone, Appl. Phys. Lett. **75**, 856 (1999).
- ²⁹ S. Li, J. A. Eastman, J. M. Vetrone, C. M. Foster, R. E. Newnham, and L. E. Cross, Jpn. J. Appl. Phys. **36**, 5169 (1997).
- ³⁰ K. J. Choi, M. Bieganski, Y. L. Li, A. Sharan, J. Schubert, R. Uecker, P. Reiche, Y. B. Chen, X. Q. Pan, V. Gopalan, L. Q. Chen, D. G. Schlom, and C. B. Eom, Science **306**, 1005 (2004).

- ³¹ J. H. Haeni, P. Irvin, W. Chang, R. Uecker, P. Reiche, Y. L. Li, S. Choudhury, W. Tian, M. E. Hawley, B. Craigo, A. K. Tagantsev, X. Q. Pan, S. K. Streiffer, L. Q. Chen, S. W. Kirchoefer, J. Levy, and D. G. Schlom, *Nature* **430**, 758 (2004).
- ³² N. A. Pertsev, A. G. Zembilgotov, and A. K. Tagantsev, *Phys. Rev. Lett.* **80**, 1988 (1998).
- ³³ O. Diéguez, K. M. Rabe, and D. Vanderbilt, *Phys. Rev. B* **72**, 144101 (2005).
- ³⁴ W. Zhong, D. Vanderbilt, and K. M. Rabe, *Phys. Rev. Lett.* **73**, 1861 (1994).
- ³⁵ W. Zhong, D. Vanderbilt, and K. M. Rabe, *Phys. Rev. B* **52**, 6301 (1995).
- ³⁶ N. A. Pertsev, A. G. Zembilgotov, and A. K. Tagantsev, *Ferroelectrics* **223**, 79 (1999).
- ³⁷ N. A. Pertsev, A. K. Tagantsev, and N. Setter, *Phys. Rev. B* **61**, R825 (2000).
- ³⁸ N. A. Pertsev, A. K. Tagantsev, and N. Setter, *Phys. Rev. B* **65**, 219901(E) (2002).
- ³⁹ N. A. Pertsev, V. G. Kukhar, H. Kohlstedt, and R. Waser, *Phys. Rev. B* **67**, 054107 (2003).
- ⁴⁰ G. Catalan, A. Jassens, G. Rispens, S. Csiszar, O. Seeck, G. Rijnders, D. H. A. Blank, and B. Noheda, *Phys. Rev. Lett.* **96**, 127602 (2006).
- ⁴¹ J. B. Neaton and K. M. Rabe, *Appl. Phys. Lett.* **82**, 1586 (2003).
- ⁴² W. Tian, J. C. Jiang, X. Q. Pan, J. H. Haeni, Y. L. Li, L. Q. Chen, D. G. Schlom, J. B. Neaton, K. M. Rabe, and Q. X. Jia, *Appl. Phys. Lett.* **89**, 092905 (2006).
- ⁴³ H. N. Lee, S. M. Nakhmanson, M. F. Chrislom, H. M. Christen, K. M. Rabe, and D. Vanderbilt, *Phys. Rev. Lett.* **98**, 217602 (2007).
- ⁴⁴ C. Ederer and N. A. Spaldin, *Phys. Rev. Lett.* **95**, 257601 (2005).
- ⁴⁵ C. Ederer and N. A. Spaldin, *Phys. Rev. B* **71**, 224103 (2005).
- ⁴⁶ W. Zhong, D. Vanderbilt, and K. M. Rabe, *Phys. Rev. B* **52**, 6301 (1995).
- ⁴⁷ Y. Umeno, T. Shimada, T. Kitamura, and C. Elsässer, *Phys. Rev. B* **74**, 174111 (2006).
- ⁴⁸ V. G. Koukhar, N. A. Pertsev, and R. Waser, *Phys. Rev. B* **64**, 214103 (2001).
- ⁴⁹ V. G. Koukhar, N. A. Pertsev, and R. Waser, *Appl. Phys. Lett.* **78**, 530 (2001).
- ⁵⁰ A. Y. Emelyanov, N. A. Pertsev, and E. K. H. Salje, *J. Appl. Phys.* **89**, 1355 (2001).
- ⁵¹ J. Paul, T. Nishimatsu, Y. Kawazoe, and U. V. Waghmare, *Phys. Rev. Lett.* **99**, 077601 (2007).
- ⁵² J. W. Matthews and A. E. Blakeslee, *J. Crys. Growth* **27**, 118 (1974).
- ⁵³ S. Gariglio, N. Stucki, J.-M. Triscone, and G. Triscone, *Appl. Phys. Lett.* **90**, 202905 (2007).
- ⁵⁴ G. Catalan, B. Noheda, J. McAneney, L. J. Sinnamon, and J. M. Gregg, *Phys. Rev. B* **72**, 020102(R) (2005).
- ⁵⁵ W. Ma and L. E. Cross, *Appl. Phys. Lett.* **88**, 232902 (2006).

- ⁵⁶ A. K. Tagantsev, Phys. Rev. B **34**, 5883 (1986).
- ⁵⁷ A. K. Tagantsev, Sov. Phys. JETP **61**, 1246 (1985).
- ⁵⁸ R. Resta, L. Colombo, and S. Baroni, Phys. Rev. B **41**, 12358 (1990).
- ⁵⁹ A. Klic and M. Marvan, Integr. Ferroelectr. **63**, 667 (2004).
- ⁶⁰ D. D. Fong, A. M. Kolpak, J. A. Eastman, S. K. Streiffer, P. H. Fuoss, G. B. Stephenson, C. Thompson, D. M. Kim, K. J. Choi, C. B. Eom, I. Grinberg, and A. M. Rappe, Phys. Rev. Lett. **96**, 127601 (2006).
- ⁶¹ J. E. Spanier, A. M. Kolpak, J. J. Urban, I. Grinberg, L. Ouyang, W. S. Yun, A. M. Rappe, and H. Park, Nano Lett. **6**, 735 (2006).
- ⁶² B. Meyer and D. Vanderbilt, Phys. Rev. B **63**, 205426 (2001).
- ⁶³ S. K. Streiffer, J. A. Eastman, D. D. Fong, C. Thompson, A. Munkholm, M. V. R. Murty, O. Auciello, G. R. Bai, and G. B. Stephenson, Phys. Rev. Lett. **89**, 067601 (2002).
- ⁶⁴ D. D. Fong, G. B. Stephenson, S. K. Streiffer, J. A. Eastman, O. Auciello, P. H. Fuoss, and C. Thompson, Science **304**, 1650 (2004).
- ⁶⁵ Ph. Ghosez and K. M. Rabe, Appl. Phys. Lett. **76**, 2767 (2000).
- ⁶⁶ I. P. Batra and B. D. Silverman, Sol. State Comm. **11**, 291 (1972).
- ⁶⁷ P. Wurfel, I. P. Batra, and J. T. Jacobs, Phys. Rev. Lett. **30**, 1218 (1973).
- ⁶⁸ I. P. Batra, P. Wurfel, and B. D. Silverman, J. Vac. Sci. Technol. **10**, 687 (1973).
- ⁶⁹ R. R. Mehta, B. D. Silverman, and J. T. Jacobs, J. Appl. Phys. **44**, 3379 (1973).
- ⁷⁰ J. Junquera and Ph. Ghosez, Nature **422**, 506 (2003).
- ⁷¹ M. Dawber, P. Chandra, P. B. Littlewood, and J. F. Scott, J. Phys.: Condens. Matter **15**, L393 (2003).
- ⁷² R. Feynman, R. B. Leighton, and M. L. Sands, *The Feynman lectures on physics* (Addison-Wesley Publishing, Reading, Massachusetts, 1989).
- ⁷³ A. Baldereschi, S. Baroni, and R. Resta, Phys. Rev. Lett. **61**, 734 (1988).
- ⁷⁴ L. Colombo, R. Resta, and S. Baroni, Phys. Rev. B **44**, 5572 (1991).
- ⁷⁵ M. Peressi, N. Binggeli, and A. Baldereschi, J. Phys. D: Appl. Phys. **31**, 1273 (1998).
- ⁷⁶ J. Junquera, M. H. Cohen, and K. M. Rabe, J. Phys.: Condens. Matter **19**, 213203 (2007).
- ⁷⁷ G. Gerra, A. K. Tagantsev, N. Setter, and K. Parlinski, Phys. Rev. Lett. **96**, 107603 (2006).
- ⁷⁸ N. Sai, A. M. Kolpak, and A. M. Rappe, Phys. Rev. B **72**, 020101 (2005).
- ⁷⁹ A. M. Bratkovsky and A. P. Levanyuk, Phys. Rev. Lett. **84**, 3177 (2000).

- ⁸⁰ A. M. Bratkovsky and A. P. Levanyuk, Phys. Rev. B **63**, 132103 (2001).
- ⁸¹ A. M. Bratkovsky and A. P. Levanyuk, Appl. Phys. Lett. **89**, 253108 (2006).
- ⁸² E. V. Chensky and V. V. Taransenko, Sov. Phys. JETP **56**, 618 (1982), [Zh. Eksp. Teor. Fiz. **83**, 1089 (1982).].
- ⁸³ M. Stengel and N. A. Spaldin, Nature **443**, 679 (2006).
- ⁸⁴ N. Sai, K. M. Rabe, and D. Vanderbilt, Phys. Rev. B **66**, 104108 (2002).
- ⁸⁵ C. Lichtensteiger, J.-M. Triscone, J. Junquera, and Ph. Ghosez, Phys. Rev. Lett. **94**, 047603 (2005).
- ⁸⁶ M. Dawber, C. Lichtensteiger, M. Cantoni, M. Veithen, Ph. Ghosez, K. Johnston, K. M. Rabe, and J.-M. Triscone, Phys. Rev. Lett. **95**, 177601 (2005).
- ⁸⁷ M. Dawber, N. Stucki, C. Lichtensteiger, S. Gariglio, Ph. Ghosez, and J.-M. Triscone, Advanced Materials (in press).
- ⁸⁸ Y. S. Kim, D. H. Kim, J. D. Kim, Y. J. Chang, T. W. Noh, J. H. Kong, K. Char, Y. D. Park, S. D. Bu, J.-G. Yoon, and J.-S. Chung, Appl. Phys. Lett. **86**, 102907 (2005).
- ⁸⁹ Y. S. Kim, J. Y. Yo, Y. J. Chang, J. H. Lee, T. W. Noh, T. K. Song, J.-G. Soon, J.-S. Chung, S. I. Baik, Y.-W. Kim, and C. U. Chung, Appl. Phys. Lett. **88**, 072909 (2006).
- ⁹⁰ L. Despont, C. Koitzsch, F. Clerc, M. G. Garnier, P. Aebi, C. Lichtensteiger, J.-M. Triscone, F. J. G. de Abajo, E. Bousquet, and Ph. Ghosez, Phys. Rev. B **73**, 094110 (2006).
- ⁹¹ J. S. Speck and W. Pompe, J. Appl. Phys. **76**, 466 (1994).
- ⁹² V. Nagarajan, J. Junquera, J. Q. He, C. L. Jia, K. Lee, Y. K. Kim, T. Zhao, Ph. Ghosez, K. M. Rabe, S. Baik, R. Waser, and R. Ramesh, J. Appl. Phys. **100**, 1 (2006).
- ⁹³ A. M. Bratkovsky and A. P. Levanyuk, Integr. Ferroelectr. **84**, 3 (2006).
- ⁹⁴ C. Lichtensteiger, M. Dawber, N. Stucki, J.-M. Triscone, J. Hoffman, J. B. Yau, C. H. Ahn, L. Despont, and P. Aebi, Appl. Phys. Lett. **90**, 052907 (2007).
- ⁹⁵ D. D. Fong, C. Cionca, Y. Yacoby, G. B. Stephenson, J. A. Eastman, P. H. Fuoss, S. K. Streiffer, C. Thompson, R. Clarke, R. Pindak, and E. A. Stern, Phys. Rev. B **71**, 144112 (2005).
- ⁹⁶ D. M. Ceperley and B. J. Alder, Phys. Rev. Lett. **45**, 566 (1980).
- ⁹⁷ J. P. Perdew and A. Zunger, Phys. Rev. B **23**, 5048 (1981).
- ⁹⁸ J. P. Perdew, J. A. Chevary, S. H. Vosko, K. A. Jackson, M. R. Pederson, D. J. Singh, and C. Fiolhais, Phys. Rev. B **46**, 6671 (1992).
- ⁹⁹ J. P. Perdew, J. A. Chevary, S. H. Vosko, K. A. Jackson, M. R. Pederson, D. J. Singh, and

- C. Fiolhais, Phys. Rev. B **48**, 4978(E) (1993).
- ¹⁰⁰ J. P. Perdew, K. Burke, and M. Ernzerhof, Phys. Rev. Lett. **77**, 3865 (1996).
- ¹⁰¹ J. P. Perdew, K. Burke, and M. Ernzerhof, Phys. Rev. Lett. **78**, 1396(E) (1997).
- ¹⁰² J. M. Soler, E. Artacho, J. D. Gale, A. García, J. Junquera, P. Ordejón, and D. Sánchez-Portal, J. Phys.: Condens. Matter **14**, 2745 (2002).
- ¹⁰³ G. Kresse and J. Hafner, Phys. Rev. B **47**, 558 (1993).
- ¹⁰⁴ G. Kresse and J. Furthmüller, Phys. Rev. B **54**, 11169 (1996).
- ¹⁰⁵ C.-G. Duan, R. F. Sabirianov, W.-N. Mei, S. S. Jaswal, and E. Y. Tsymbal, Nano Lett. **6**, 483 (2006).
- ¹⁰⁶ See the DTU web page: <https://wiki.fysik.dtu.dk/dacapo>.
- ¹⁰⁷ B. Meyer, F. Lechermann, C. Elsässer, and M. Fähle, Fortran90 Program for Mixed-Basis Pseudopotential Calculations for Crystals (Max-Planck-Institut für Metallforschung, Stuttgart).
- ¹⁰⁸ Y. Umeno, B. Meyer, C. Elsässer, and P. Gumbsch, Phys. Rev. B **74**, 060101(R) (2006).
- ¹⁰⁹ N. Sai, A. M. Kolpak, and A. M. Rappe, Phys. Rev. B **74**, 059901(E) (2006).
- ¹¹⁰ G. Gerra, A. K. Tagantsev, and N. Setter, Phys. Rev. Lett. **98**, 207601 (2007).
- ¹¹¹ M. Stengel, and N. Spaldin, Phys. Rev. B **75**, 205121 (2007).
- ¹¹² A. M. Kolpak, N. Sai, and A. M. Rappe, Phys. Rev. B **74**, 054112 (2006).
- ¹¹³ A. M. Kolpak, N. Sai, and A. M. Rappe, Phys. Rev. B **74**, 099901(E) (2006).
- ¹¹⁴ Z. Wu, R. E. Cohen, and D. J. Singh, Phys. Rev. B **70**, 104112 (2004).
- ¹¹⁵ D. Bilc, R. Schaltaf, G.-M. Rignanese, J. Íñiguez, and Ph. Ghosez, unpublished.
- ¹¹⁶ Z. Wu and R. E. Cohen, Phys. Rev. B **73**, 235116 (2006).
- ¹¹⁷ J. Junquera, M. Zimmer, P. Ordejón, and Ph. Ghosez, Phys. Rev. B **67**, 155327 (2003).
- ¹¹⁸ J. P. Velez, C. G. Duan, K. D. Belashchenko, S. S. Jaswal, and E. Y. Tsymbal, Phys. Rev. Lett. **98**, 137201 (2007).
- ¹¹⁹ S. Tinte and M. G. Stachiotti, in *Fundamental Physics of Ferroelectrics 2000*, edited by R. E. Cohen, AIP Conf. Proc. **535** (AIP, Woodbury, 2000), pp. 273–283.
- ¹²⁰ S. Tinte and M. G. Stachiotti, Phys. Rev. B **64**, 235403 (2001).
- ¹²¹ M. G. Stachiotti, Appl. Phys. Lett. **84**, 251 (2004).
- ¹²² Y. H. Shin, I. Grinberg, I. W. Chen, and A. M. Rappe, Nature **449**, 881 (2007).
- ¹²³ Z. Wu, N. Huang, Z. Liu, J. Wu, W. Duan, B. L. Gu, and X. W. Zhang, Phys. Rev. B **70**, 104108 (2004).

- ¹²⁴ Z. Wu, N. Huang, J. Wu, W. Duan, and B.-L. Gu, Appl. Phys. Lett. **86**, 202903 (2005).
- ¹²⁵ I. Kornev, H. Fu, and L. Bellaiche, Phys. Rev. Lett. **93**, 196104 (2004).
- ¹²⁶ I. Ponomareva, I. I. Naumov, I. Kornev, H. Fu, and L. Bellaiche, Phys. Rev. B **72**, 140102(R) (2005).
- ¹²⁷ I. Ponomareva, I. I. Naumov, and L. Bellaiche, Phys. Rev. B **72**, 214118 (2005).
- ¹²⁸ B.-K. Lai, I. Ponomareva, I. I. Naumov, I. Kornev, H. Fu, L. Bellaiche, and G. J. Salamo, Phys. Rev. Lett. **96**, 137602 (2006).
- ¹²⁹ B.-K. Lai, I. Ponomareva, I. A. Kornev, L. Bellaiche, and G. J. Salamo, Phys. Rev. B **75**, 085412 (2007).
- ¹³⁰ L. Landau and E. Lifshitz, Phys. Z. Sowjetunion **8**, 153 (1935).
- ¹³¹ C. Kittel, Phys. Rev. **70**, 965 (1946).
- ¹³² C. Kittel, Rev. Mod. Phys. **21**, 541 (1949).
- ¹³³ J. F. Scott, unpublished.
- ¹³⁴ S. Prosandeev and L. Bellaiche, Phys. Rev. B **75**, 172109 (2007).
- ¹³⁵ G. B. Stephenson and K. R. Elder, J. Appl. Phys. **100**, 051601 (2006).
- ¹³⁶ P. Aguado-Puente and J. Junquera, unpublished.
- ¹³⁷ B.-K. Lai, I. Ponomareva, I. Kornev, L. Bellaiche, and G. J. Salamo, Appl. Phys. Lett. **91**, 152909 (2007).
- ¹³⁸ E. Almahmoud, Y. Navtsenya, I. Kornev, H. Fu, and L. Bellaiche, Phys. Rev. B **70**, 220102(R) (2004).
- ¹³⁹ I. Ponomareva and L. Bellaiche, Phys. Rev. B **74**, 064102 (2006).
- ¹⁴⁰ Th. Tybell, P. Paruch, T. Giamarchi, and J.-M. Triscone, Phys. Rev. Lett. **89**, 097601 (2002).
- ¹⁴¹ G. Rijnders and D. H. A. Blank, Nature **433**, 369 (2005).
- ¹⁴² H. Iijima, T. Terashima, Y. Bando, K. Kamigaki, and H. Terauchi, J. Appl. Phys. **72**, 2840 (1992).
- ¹⁴³ H. Tabata, H. Tanaka, and T. Kawai, Appl. Phys. Lett. **65**, 1970 (1994).
- ¹⁴⁴ H. Tabata and T. Kawai, Appl. Phys. Lett. **70**, 321 (1997).
- ¹⁴⁵ T. Zhao, Z. H. Chen, F. Chen, W. S. Shi, H. B. Lu, and G. Z. Yang, Phys. Rev. B **60**, 1697 (1999).
- ¹⁴⁶ T. Tsurumi, T. Ichikawa, T. Harigai, H. Kakemoto, and S. Wada, J. Appl. Phys. **91**, 2284 (2002).

- ¹⁴⁷ T. Shimuta, O. Nakagawara, T. Makino, S. Arai, H. Tabata, and T. Kawai, *J. Appl. Phys.* **91**, 2290 (2004).
- ¹⁴⁸ A. Q. Jiang, J. F. Scott, H. Lu, and Z. Chen, *J. Appl. Phys.* **93**, 1180 (2003).
- ¹⁴⁹ S. Ríos, A. Ruediger, A. Q. Jiang, J. F. Scott, H. Lu, and Z. Chen, *J. Phys.: Condens. Matter* **15**, L305 (2003).
- ¹⁵⁰ K. Johnston, X. Huang, J. B. Neaton, and K. M. Rabe, *Phys. Rev. B* **71**, 100103(R) (2005).
- ¹⁵¹ J. Lee, L. Kim, J. Kim, D. Jung, and U. V. Waghmare, *J. Appl. Phys.* **100**, 051613 (2006).
- ¹⁵² D. A. Tenne, A. Bruchhausen, N. D. Lanzillotti-Kimura, A. Fainstein, R. S. Katiyar, A. Cantarero, A. Soukiassian, V. Vaithyanathan, J. H. Haeni, W. Tian, D. G. Schlom, K. J. Choi, D. M. Kim, C. B. Eom, H. P. Sun, X. Q. Pan, Y. L. Li, L. Q. Chen, Q. X. Jia, S. M. Nakhmanson, K. M. Rabe, X. X. Xi, and *Science* **313**, 1614 (2006).
- ¹⁵³ S. Lisenkov and L. Bellaiche, *Phys. Rev. B* **76**, 020102(R) (2007).
- ¹⁵⁴ J. C. Jiang, X. Q. Pan, W. Tian, C. D. Theis, and D. G. Schlom, *Appl. Phys. Lett.* **74**, 2851 (1999).
- ¹⁵⁵ E. Bousquet and Ph. Ghosez, unpublished.
- ¹⁵⁶ E. D. Specht, H. M. Christen, D. P. Norton, and L. A. Boatner, *Phys. Rev. Lett.* **80**, 4317 (1998).
- ¹⁵⁷ M. Sepliarsky, S. R. Phillpot, D. Wolf, M. G. Stachiotti, and R. L. Migoni, *Phys. Rev. B* **64**, R060101 (2001).
- ¹⁵⁸ M. Sepliarsky, S. R. Phillpot, D. Wolf, M. G. Stachiotti, and R. L. Migoni, *J. Appl. Phys.* **90**, 4509 (2001).
- ¹⁵⁹ M. Sepliarsky, S. R. Phillpot, M. G. Stachiotti, and R. L. Migoni, *J. Appl. Phys.* **91**, 3165 (2002).
- ¹⁶⁰ H. N. Lee, H. M. Christen, M. F. Chisholm, C. M. Rouleau, and D. H. Lowndes, *Nature* **433**, 395 (2005).
- ¹⁶¹ S. M. Nakhmanson, K. M. Rabe, and D. Vanderbilt, *Appl. Phys. Lett.* **87**, 102906 (2005).
- ¹⁶² S. M. Nakhmanson, K. M. Rabe, and D. Vanderbilt, *Phys. Rev. B* **73**, 060101(R) (2006).
- ¹⁶³ T. Tsurumi, T. Harigai, D. Tanaka, S.-M. Nam, H. Kakemoto, S. Wada, and K. Saito, *Appl. Phys. Lett.* **85**, 5016 (2004).
- ¹⁶⁴ X. Wu, O. Diéguez, K. M. Rabe, and D. Vanderbilt, *Phys. Rev. Lett.* **97**, 107602 (2006).
- ¹⁶⁵ V. A. Stephanovich, I. A. Lukyanchuk, and M. G. Karkut, *Phys. Rev. Lett.* **94**, 047601 (2005).

- 166 A. M. George, J. Íñiguez, and L. Bellaiche, *Nature* **413**, 54 (2001).
- 167 N. Huang, Z. Liu, Z. Wu, J. Wu, W. Duan, B. L. Gu, and X. W. Zhang, *Phys. Rev. Lett.* **91**, 067602 (2003).
- 168 I. A. Kornev and L. Bellaiche, *Phys. Rev. Lett.* **91**, 116103 (2003).
- 169 N. Sai, B. Meyer, and D. Vanderbilt, *Phys. Rev. Lett.* **84**, 5636 (2000).
- 170 J. Íñiguez and L. Bellaiche, *Phys. Rev. Lett.* **87**, 095503 (2001).
- 171 W. S. Yun, J. J. Urban, Q. Gu, and H. Park, *Nano Lett.* **2**, 447 (2002).
- 172 Z. Wang, A. P. Suryavanshi, and M. F. Yu, *Appl. Phys. Lett.* **89**, 082903 (2006).
- 173 Y. Luo, I. Szafraniak, N. D. Zakharov, V. Nagarajan, M. Steinhart, R. B. Wehrspohn, R. Ramesh, and M. Alexe, *Appl. Phys. Lett.* **83**, 440 (2003).
- 174 F. D. Morrison, Y. Luo, I. Szafraniak, V. Nagarajan, R. B. Wehrspohn, M. Steinhart, J. H. Wendroff, N. D. Zakharov, E. D. Mishina, K. A. Vorotilov, A. S. Sigov, M. Alexe, R. Ramesh, and J. F. Scott, *Rev. Adv. Mater. Sci* **4**, 114 (2003).
- 175 A. Schilling, R. M. Bowman, J. M. Gregg, G. Catalan, and J. F. Scott, *Appl. Phys. Lett.* **89**, 212902 (2006).
- 176 M.-W. Chu, I. Szafraniak, R. Scholz, C. Harnagea, D. Hesse, M. Alexe, and U. Gosele, *Nat. Mater.* **3**, 87 (2004).
- 177 X. H. Zhu, P. R. Evans, D. Byrne, A. Schilling, C. Douglas, R. J. Pollard, R. M. Bowman, J. M. Gregg, F. D. Morrison, and J. F. Scott, *Appl. Phys. Lett.* **89**, 122913 (2006).
- 178 H. Fu and L. Bellaiche, *Phys. Rev. Lett.* **91**, 257601 (2003).
- 179 I. I. Naumov, L. Bellaiche, and H. X. Fu, *Nature* **432**, 737 (2004).
- 180 J. F. Scott, *Nat. Mater.* **4**, 13 (2005).
- 181 S. Prosandeev, I. Ponomareva, I. Kornev, I. Naumov, and L. Bellaiche, *Phys. Rev. Lett.* **96**, 237601 (2006).
- 182 S. Prosandeev and L. Bellaiche, *Phys. Rev. Lett.* **97**, 167601 (2006).
- 183 I. Naumov and H. Fu, *Phys. Rev. Lett.* **98**, 077603 (2007).
- 184 J. Wang and T.-Y. Zhang, *Appl. Phys. Lett.* **88**, 182904 (2006).
- 185 I. I. Naumov and H. Fu, *Phys. Rev. Lett.* **95**, 247602 (2005).
- 186 G. Geneste, E. Bousquet, J. Junquera, and Ph. Ghosez, *Appl. Phys. Lett.* **88**, 112906 (2006).
- 187 G. Geneste, E. Bousquet, and Ph. Ghosez, *Journal of Theoretical and Computational Nanoscience*, (in press).

- ¹⁸⁸ P. Paruch, T. Giamarchi, and J.-M. Triscone, Phys. Rev. Lett. **94**, 197691 (2005).
- ¹⁸⁹ P. Paruch, T. Giamarchi, Th. Tybell, and J.-M. Triscone, J. Appl. Phys. **100**, 051608 (2006).
- ¹⁹⁰ P. Paruch, T. Giamarchi, and J.-M. Triscone, Topics Appl. Physics **105**, 339 (2007).
- ¹⁹¹ M. Y. Zhuravlev, R. F. Sabirianov, S. S. Jaswal, and E. Y. Tsymbal, Phys. Rev. Lett. **94**, 246802 (2005).
- ¹⁹² E. Y. Tsymbal and H. Kohlstedt, Science **313**, 181 (2006).
- ¹⁹³ C.-G. Duan, S. S. Jaswal, and E. Y. Tsymbal, Phys. Rev. Lett. **97**, 047201 (2006).
- ¹⁹⁴ S. Sahoo, S. Polisetty, C. D. Duan, S. S. Jaswal, E. Y. Tsymbal, and C. Binek, Phys. Rev. B **76**, 092108 (2007).
- ¹⁹⁵ A. J. Hatt and N. A. Spaldin, Appl. Phys. Lett. **07**, 242916 (2007).